



27 discovered in subsequent years, forming “families” of baryons and mesons. Some of them  
28 had unexpectedly long lifetimes, which was the first hint to the existence of “quarks” as  
29 a *substructure* of hadrons. A new type of quark, called “strange”, not present in stable  
30 matter, was considered as causing the long lifetime of those particles.

31 The mass scale of newly detected particles seemed to have no obvious upper limit. To open  
32 the window for the discovery of ever heavier particles, the Super Proton Synchrotron (SPS)  
33 was constructed at CERN, starting 1972, with a maximum energy of 400 GeV. Due to the  
34 kinematics of a proton hitting another proton at rest (like in a stationary hydrogen target),  
35 an increase of beam energy does not lead to a proportional increase of the energy available  
36 for the collision process, because the energy in the Center of Momentum System (CMS)  
37 only grows with the square root of the beam energy. If, in contrast, the two particles  
38 collided “head-on”, the energy in the CMS would be twice the beam energy. This led  
39 to the colliding beam concept for High Energy physics experiments, where two beams,  
40 circulating in opposite direction, are brought to collide at predefined interaction regions  
41 (IA), where, subsequently, the collision products can be observed in detectors surrounding  
42 the IA region. In order to explore this concept, a pioneering p-p collider, the Intersecting  
43 Storage Rings (ISR) were built at CERN, starting to operate in 1971. The CMS energy  
44 was twice the injection energy from the PS, i.e. 60 GeV. Compared to this, the 400 GeV  
45 beam energy on proton targets, as produced by the SPS, could only provide a CMS energy  
46 of 20 GeV.

47 Historically, the colliding beam technique was pioneered in collisions between electrons and  
48 positrons ( $e^+ - e^-$ ), because a number of technical aspects helped to facilitate the operation  
49 of  $e^+ - e^-$  compared to p-p colliders. Pioneering  $e^+ e^-$  colliders were built at the Italian  
50 National Laboratory for Particle Physics (ADONE), at the Stanford Linear Accelerator  
51 Center (SPEAR) and at DESY near Hamburg (DORIS), providing CMS energies of 3, 4  
52 and 8 GeV, respectively. At SPEAR, the  $J/\psi$  meson was discovered in 1974 and confirmed  
53 at DORIS, which established the existence of the *charmed* quark, partner of the *strange*  
54 quark in the second quark generation. A more powerful  $e^+e^-$  collider, with an energy of  
55 up to 24 GeV per beam (PETRA), was built at DESY, starting to operate in 1978. It was  
56 the first collider, where gluons were identified in events with three well-separated hadron  
57 jets.

58 The fact that  $e^+$  and  $e^-$  are of opposite charge allows both beams to circulate in the same  
59 magnetic field, requiring only one vacuum ring, which leads to an important simplification  
60 of the technical implementation. Thus, when anti-proton cooling was invented at CERN  
61 in 1976, it appeared that the SPS could be used in the same operation mode, proton and  
62 anti-proton being of opposite charge. The SPS was therefore converted into a colliding  
63 beam machine, reaching 540 GeV energy in the CMS system, by far the highest energy  
64 achieved by that time. It allowed, late in 1983, to prove the existence of the  $W^{+/-}$  and  
65  $Z^0$  bosons, which is one of the highlights in the history of CERN.

66 In the wake of this success, a series of new collider projects was initiated. At CERN, the  
67 Large Electron Positron collider (LEP) was built to reach twice 100 GeV and to become a  
68 “discovery machine” as well as a “factory” for the production of Z and W bosons. After  
69 the termination of the LEP project, anticipated for 2001, the LEP tunnel became free for



| Laboratory | Collider name | Time of operation | Particle types   | Beam energies GeV * GeV | Experiment w. MPP involvement |
|------------|---------------|-------------------|------------------|-------------------------|-------------------------------|
| DESY       | DORIS         | 1974-2013         | $e^+ e^-$        | 5 * 5                   | DASP                          |
| DESY       | PETRA         | 1978-1986         | $e^+ e^-$        | 24 * 24                 | CELLO (JADE)                  |
| CERN       | LEP           | 1989-2000         | $e^+ e^-$        | 104 * 104               | Aleph (OPAL)                  |
| DESY       | HERA          | 1992-2007         | $e^\pm p$        | 30 * 920                | H1                            |
| BNL        | RHIC          | 2000-now          | $p^* \text{Ion}$ | 255 * 100/n             | STAR                          |
| KEK        | SuperKEKB     | 2016-now          | $e^+ e^-$        | 4 * 7                   | Belle II                      |
| CERN       | LHC           | 2008-now          | $p p$            | 6800 * 6800             | ATLAS                         |

Table 1: Collider projects with substantial MPP participation. For the beam energies the maximally reached values are given. The projects in brackets came to the MPP in 2000 with the new director Prof. Bethke.

70 a powerful new p-p collider, planned to operate at  $2 \times 7 \text{ TeV}$ , called the Large Hadron  
71 Collider (LHC).

72 All along the rapid development of particle colliders to ever higher CMS energies, MPP  
73 took a leading role in planning, testing and constructing experimental facilities, able to  
74 cope with increasing requirements for energy resolution, tracking accuracy, angular accep-  
75 tance and readout speed. Two big experiments with MPP leadership were constructed  
76 and operated at the PETRA and HERA colliders at DESY. Using sampling calorimeters  
77 in a Liquid Argon medium (LAr), the detection of neutral particles and hadronic jets was  
78 brought to a high level of perfection and reliability. Table 1 gives an overview of major  
79 MPP experiments at colliders.

80 At CERN, MPP was one of the main proponents of the ALEPH experiment at LEP, where  
81 the institute contributed two novel technologies for particle tracking. Thus, from the very  
82 beginning, MPP took a leading role in design and construction of the Time Projection  
83 Chamber (TPC), in particular in the development of the complex structures of the end  
84 plate with demanding requirements for mechanical accuracy and reliability of the TPC  
85 as well as for the high level of timing accuracy of the readout electronics. MPPs second,  
86 crucial contribution to tracking was the Silicon Strip detector, allowing to measure tracks  
87 with the unprecedented accuracy of about  $10 \mu\text{m}$ . This way, secondary vertices could be  
88 identified, which were displaced from the beam interaction point by a very short distance,  
89 a key feature to identify decays of B-mesons. Based on this capacity, ALEPH became  
90 leader in the exploration of B-physics at LEP. The experience gained with the ALEPH  
91 TPC was later used in the STAR experiment at the RHIC collider (Relativistic Heavy  
92 Ion Collider) at BNL, where MPP contributed a new type of TPC, optimized for the very  
93 forward region.

94 While LEP went into operation at CERN, a special form of collider was constructed  
95 at DESY, allowing collisions between protons and electrons at the HERA storage rings.  
96 MPP was responsible for calorimetry in the H1 experiment as well as for a new strategy of  
97 trigger formation with Neural Networks. The calorimeter at H1, based on LAr technology,  
98 achieved the planned energy resolution and demonstrated high reliability during operation.

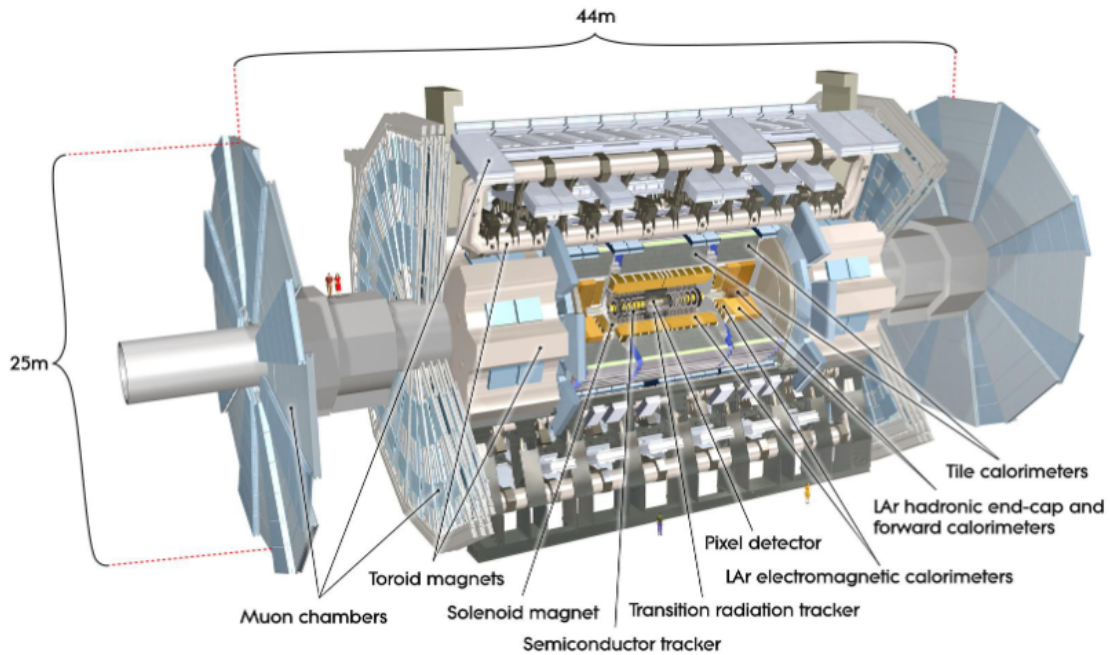


Figure 1: Cutaway view of the ATLAS detector with the central tracking detector (see chapter 2), the calorimeters (see chapter 3), and, surrounding everything else, the central cylindrical (barrel) and the endcap parts of the muon spectrometer with their separate superconducting toroid magnet systems. The precision muon tracking chambers (MDT) constructed at MPP (see chapter 4) are located in the outermost layer of the central cylindrical (barrel) part, mounted on the outside of the eight superconducting barrel toroid magnet coils, as indicated in the picture.

99 While LEP was in the final phase of construction, CERN vigorously pursued planning and  
 100 prototyping for the follow-up project LHC. In parallel, on the side of the experimenters,  
 101 work on detector concepts was taking shape. MPP proposed a detector type with the  
 102 unique feature of a superconducting magnet with toroidal geometry (ASCOT), which did  
 103 not use an iron core and – for this reason – was nearly transparent for muon particles  
 104 emerging from the interaction point. When the ASCOT proposal was finally merged with  
 105 another project - EAGLE - to become ATLAS, the iron-free magnet design was adopted,  
 106 because the accuracy of muon tracking was one of the crucial requirements for a potential  
 107 observation of the Higgs particle.

108 When the LHC became reality, planning for ATLAS entered a new phase. MPP played a  
 109 crucial role in defining the technology in three subdetectors:

- 110 • The Inner Detector (ID) had to measure particle tracks with high accuracy in a  
 111 background rate of about  $10^9$  particles per second. In the innermost region, close to  
 112 the beam pipe, this could only be done by Silicon Strip detectors, and MPP, based  
 113 on the experience at LEP, led the development of detectors as well as the design of  
 114 efficient readout strategies.

- 115 • The Endcap calorimeters for the precise measurement of hadronic showers were  
116 designed and built by MPP, in collaboration with other institutes.
- 117 • The Superconducting Toroidal magnets in the voluminous outer region had to be  
118 equipped with muon detectors with very high spatial resolution, covering about  
119  $5000 m^2$ . MPP conceived a novel concept for particle tracking, the Monitored Drift  
120 Tube technology (MDT), combining high accuracy of tracking and alignment, ro-  
121 bustness in operation and cost-effectiveness of production.

122 At present, the LHC being in its 15th year of operation, the technical concepts developed  
123 by MPP have proven to completely match or exceed expectations.

124 Even before the LHC went into operation (2008), ideas for a luminosity upgrade of the LHC  
125 were discussed, which resulted in the construction of the High-Luminosity LHC (HL-LHC).  
126 A luminosity increase by an order of magnitude beyond the one of the “original” LHC  
127 ( $10^{34} cm^{-2} s^{-1}$ ) was conceived. An upgrade at this scale, however, meant a big challenge  
128 to experimenters, as increased data recording capabilities and higher detector granularity  
129 were required for the various subdetectors of ATLAS. Among other technical requirements,  
130 a new trigger concept with higher latency was needed as well as a significantly higher  
131 bandwidth for data processing and readout, which, in consequence, lead to the necessity  
132 of a complete renewal of the readout electronics in all subdetectors. Detector elements,  
133 exposed to high particle rates or radiation doses, would have to be replaced by devices  
134 with higher hit capability, granularity and radiation tolerance.

135 As for the muon tracking detectors, drift tube detectors with smaller tube diameter  
136 (sMDT) were developed to provide eight times higher rate capability. In a sequence  
137 of development steps, a series of constantly improved sMDT chambers was added to the  
138 existing ATLAS structure, in such a way as to test the new technology under real ex-  
139 perimental conditions. The complete Inner Detector of ATLAS will be replaced by an  
140 all-Silicon barrel tracker with finer granularity and higher radiation tolerance. At the  
141 time of this article, work for the upgrade to the HL-LHC is in full swing and driven by a  
142 fixed production and installation schedule.

143 The future of highest energy particle colliders beyond the HL-LHC is a matter of intense  
144 discussion since a long time and not yet fully clarified. The Future Circular Collider  
145 (FCC) project promoted at CERN is a large  $e^+ e^-$  collider of about 90 km circumference  
146 to be used as a “Higgs factory” (FCC-ee), to be followed by a pp collider in the same  
147 tunnel with around 100 TeV collision energy. In all scenarios of future colliders, detectors  
148 with high granularity, high spatial and energy resolution will be needed, being able to  
149 work at high particle rates and high radiation levels. The MPP is well prepared for this  
150 scenario, taking advantage of its long-standing experience in detector design, realization  
151 and operation.

## 152 **3 Vertexing: Pioneering Silicon Detectors**

### 153 **3.1 Silicon Detectors in High Energy Physics**

154 The Max Planck Institute for Physics has been playing a leading rôle developing silicon  
155 detectors for applications in High Energy Physics. This started in the seventies when the  
156 MPP physicists Gerhard Lutz and Robert Klanner, together with Josef Kemmer from the  
157 TUM, developed the first useful silicon strip detectors for fixed target experiments.

158 If precision, compactness, and speed is required silicon is the detector material of choice. In  
159 silicon about 3.6 eV of energy loss is needed to create an electron hole pair, the ionization  
160 energy in gases is in the order of 15 eV for argon and even higher for other gases. In  
161 addition the ionization density is higher: a minimum ionizing particle creates 800,000  
162 electron hole pairs per cm in silicon but only 100 electrons per cm are created in a gas  
163 like argon. The signals in silicon can be amplified directly with charge sensitive amplifiers.  
164 No high fields for gas amplification are needed. Hence comfortably large signals can be  
165 obtained in very thin layers of silicon. Because of this and the possibility to pattern the  
166 detectors very finely using photolithography a superior position resolution can be achieved.

167 Silicon detectors had their first appearance in High Energy Physics in the seventies when  
168 high precision vertex detectors were needed for lifetime measurements of the recently dis-  
169 covered charmed particles. Lifetimes in the picosecond range required a spatial resolution  
170 of a few  $10\ \mu\text{m}$  in order to resolve the decay vertex from the production vertex. Bubble  
171 chambers and emulsions, which could in principle achieve such a resolution, could not  
172 cope with large data rates. Gaseous detectors were fast, but not precise enough. Silicon  
173 detectors could be segmented fine enough to provide sufficient resolution at the required  
174 speed.

175 However, first a series of technical problems had to be overcome. The breakthrough was  
176 the introduction of the planar process by J. Kemmer [1] which made it possible to construct  
177 high quality detectors, replacing the surface barrier technology proposed earlier [2]. The  
178 ACCMOR collaboration (**A**msterdam, **C**racow, **C**ERN, **M**unich, **O**xford, **R**utherford)  
179 operating the NA11 (1978-1982) and NA32 (1982-1986) experiments [3] at CERN were  
180 the first to use these silicon strip detectors. The readout electronics was bulky and had  
181 to be connected to the detectors using large fan-out boards as shown in Fig. 2. Hence the  
182 use of silicon detectors was limited to fixed target experiments with their telescope-like  
183 detectors. These experiments made important contributions to the measurement of the  
184 lifetimes of charmed Mesons [4] and Baryons [5].

#### 185 **3.1.1 Vertex Detectors at LEP: ALEPH (1989-2000)**

186 In order to use silicon strip sensors in the upcoming LEP experiments with their  $4\pi$   
187 detectors miniature electronics was needed which could allow a direct coupling of an  
188 amplifier to a silicon strip requiring a width of the amplifier of  $O(100\ \mu\text{m})$ . The introduction



Figure 2: Photo of the first silicon strip detector made in planar technology. This detector was used in the NA11/NA32 experiment. The sensor's sensitive area is  $24 \times 36 \text{ mm}^2$ . The sensor is embedded in a large fan out board providing cable connections to individual amplifiers.

189 of VLSI (**V**ery **L**arge **S**cale **I**ntegration) electronics made it possible to construct compact  
190 silicon detectors which could be installed in colliding beam experiments. One of the first  
191 VLSI chips for silicon strip detector readout was the CAMEX64 [6] developed at MPP  
192 and the Fraunhofer Institute in Duisburg by Gerhard Lutz for the ALEPH experiment.

193 MPP was member of the ALEPH collaboration (and played a leading role in the con-  
194 struction of the superb TPC (**T**ime **P**rojection **C**hamber)) and, together with INFN Pisa,  
195 constructed the first Vertex detector using double sided silicon strip detectors [7]. Pisa  
196 originally proposed a silicon vertex detector using single sided detectors, however. MPP  
197 joined the proposal extending it to the use of double sided detectors.

198 Simple single sided strip sensors measure only one coordinate of a track. This matches the  
199 resolution of the outer (gaseous) tracking detectors where high resolution is only needed  
200 in the bending plane of the magnetic field. However, the tracks of decaying particles are  
201 distributed isotropically in  $r - \phi$  and  $z$  and a projective measurement results in a loss of  
202 information and precision. Measuring two coordinates of a track with rotated strips pro-  
203 vides a two-dimensional measurement, improving the possibilities of vertex reconstruction.  
204 This can be achieved by rotating the strip directions in different sensor planes resulting in  
205 a kind of stereo view. One step further is a real double sided detector: both surfaces of a  
206 sensor are instrumented collecting either electrons or holes, again with the strip directions  
207 rotated. One disadvantage of such stereo arrangements are association ambiguities in case  
208 more than one track traverses the detector. At LEP the track density was low enough so  
209 that there was no severe limitation due to these ambiguities. A further complication is the  
210 double sided processing required for such detectors. In standard single sided detectors the  
211 backside of the silicon wafer needs, besides a homogeneous implant and passivation, no  
212 further processing, making the handling during production rather easy. In double sided

213 detectors the back side needs to be patterned as well introducing many complications in  
 214 the production process. First trials to produce such detectors in the laboratory of Josef  
 215 Kemmer at MBB delivered prototypes demonstrating that such detectors could work but  
 216 failed to produce detectors with high production yield and 100% strip efficiency. Finally we  
 217 found with CSEM in Neuchatel a company able to produce such detectors according to our  
 218 specifications. ALEPH was the first experiment to use double sided silicon sensors. Other  
 219 features of the sensors were the punch-through biasing of the p-strips and the use of the  
 220 electron accumulation layer as bias resistor on the n-side. The detectors were DC-coupled.  
 221 AC coupling to the amplifier was made using special capacitor ASICs bonded between the  
 222 strips and the amplifiers. This reflected the initial difficulty to produce AC-coupled sensors  
 223 with high yield. Separating the AC coupling to an external, cheap and testable AC chip  
 224 was a cost effective solution despite some complication for module construction. Another  
 225 problem was the placement of the readout ASICs for the strips measuring the z-coordinate  
 226 (along the beam). ALEPH placed them along the detector which resulted in an increase  
 227 of material. Nevertheless the total amount of material of the two layer detector was only  
 228  $3\% X_0$  (average) for orthogonal tracks.

229 Altogether the way to go was long and difficult and not without tensions between the Pisa  
 230 and MPP groups. Many components had to be designed basically from scratch without  
 231 prior experience, like lightweight but rigid mechanical structures, fine pitch ceramic hy-  
 232 brids. We also had to learn how to do fine pitch wire bonding. The original design foresaw  
 233 the detector to be fixed on the beam pipe, therefore being the first subdetector to be  
 234 installed. Delays in construction and schedule constraints made this very soon impossible.  
 235 Instead we developed a method to install the mini vertex later by use of a kind of ropeway  
 236 which allowed to drag the detector in its position, defined by rails, from the outside. In  
 237 1989 a first prototype was installed consisting only of three modules. It performed very  
 238 badly suffering from huge common mode noise caused by beam pick up which could not  
 239 be compensated. In 1990 a new vertex detector was installed in ALEPH (Fig. 3). Despite  
 240 various improvement it still showed poor performance, however could be tuned to deliver  
 241 useful data. Unfortunately the detector was partially destroyed by a beam accident. We  
 242 started to construct a new detector essentially from scratch to be ready in 1991. In the  
 243 meantime LEP proposed to replace the rather large beam pipe of LEP (radius: 7.8 cm),  
 244 which resulted in a large extrapolation error, by a smaller one. The radius was reduced  
 245 to 5.3 cm and the new vertex detector could be placed closer to the beam.

246 This detector had two layers at radii of 6.3 cm and 10.9 cm and achieved a position  
 247 resolution of  $12\mu$ . The vertex detector proved to be an indispensable part of the ALEPH  
 248 detector systems, contributing to many measurements. Among them were precise mea-  
 249 surements of the inclusive lifetime of B-hadrons [8], the individual lifetimes of  $B^0$ ,  $B^+$ ,  
 250  $B_s$  mesons and b-baryons [9, 10, 11]. The first direct measurement of  $B^0\bar{B}^0$ -oscillation  
 251 frequency was performed by ALEPH [12]. The Mini vertex was the decisive detector for  
 252 the precision measurement of the branching fraction  $Z \rightarrow b\bar{b}$ : Using impact parameter  
 253 tagging it was possible to select pure samples of B-events with high efficiency [13]. A nice  
 254 example of the power of the vertex detector is a fully reconstructed  $B_s^0$  decay observed  
 255 in the ALEPH detector (Fig. 4). The secondary and tertiary vertices of the  $B_s \rightarrow D_s\pi$   
 256 decay chain are nicely resolved. This illustrates how B-mesons can be reconstructed and  
 257 lifetimes measured. Such fully reconstructed events are rare, ALEPH reconstructed only

258 one in  $11 \times 10^6$  Z events, therefore mostly partially reconstructed events are used in the  
259 analysis, e.g. with neutral particles missing.

260 ALEPH and DELPHI had silicon strip detectors right from the beginning. The other two  
261 LEP experiments, OPAL and L3 joined the silicon club later.

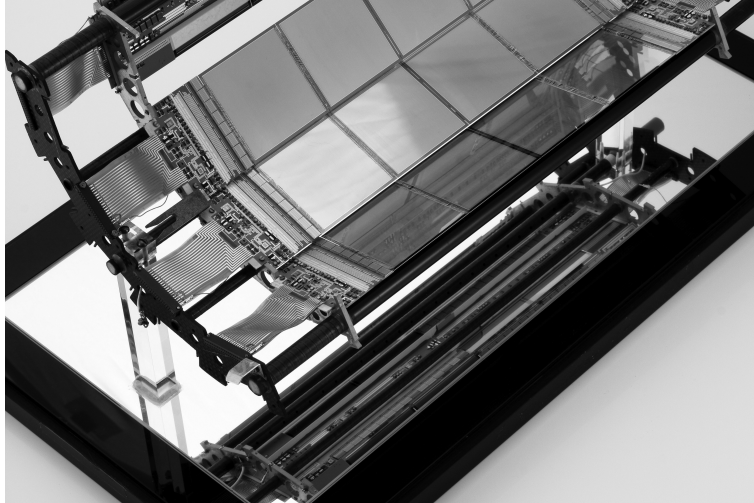


Figure 3: Photo of a sector of the first ALEPH silicon vertex detector. The detector was divided in three sectors, each housing two layers of four modules each. Three of the inner layer modules are shown, one is removed to show the z-side of a module of the second layer. This detector was the first using double sided silicon strip sensors and was used in the 1990 ALEPH run. It was replaced 1991 by a new detector with smaller inner radius. The dimensions of the silicon sensors are  $52 \times 52 \text{ mm}^2$ .

### 262 3.2 The Semiconductor Laboratory: HLL

263 After the experience with ALEPH it became evident that the optimal development and  
264 production of high quality silicon detectors needs a special, dedicated laboratory with  
265 production facilities. While collaboration with industry is in principle possible, it in-  
266 troduce severe boundary conditions which hamper innovation. Industrial processes are  
267 usually optimized for low cost mass production. Special processing needed for our detec-  
268 tors are either not available or the company is reluctant to adopt the process parameters  
269 to our needs. Often these parameters are not disclosed which makes it very difficult to  
270 optimize the design of the detectors. Fortunately, our colleagues from the Max Planck  
271 Institute for Extraterrestrial Physics faced the same problem developing silicon detectors  
272 for X-ray imaging. Both institutes joined to found a common semiconductor laboratory  
273 (**H**albleiterlabor: HLL) in 1990.

274 The lab was located in Pasing, in rooms used by the Fraunhofer Institut für Festkörpertechnologie  
275 before. It included  $250 \text{ m}^2$  of a class 10-100 cleanroom equipped for processing of 4 inch  
276 wafers. This was completed by test facilities and office space for design, analysis and

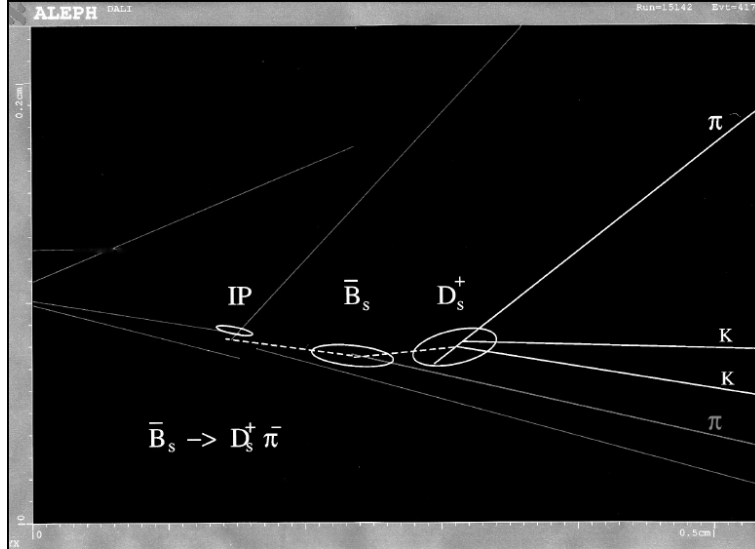


Figure 4: A  $\bar{B}_s$  decaying into a  $D_s^+ \pi^-$  with the subsequent decay of the  $D_s^+$  into a  $\pi^+$  and two oppositely charged Kaons fully reconstructed in the ALEPH detector. The error ellipses ( $3\sigma$ ) of the interaction point (IP) and two decay vertices are indicated. All tracks are extrapolation of tracks measure in the vertex detector. The  $\bar{B}_s$  decayed after 1.57 mm, the  $D_s^+$  at 2.71 mm from the IP.

277 administration. The lab was very successful, the pn-CCDs for the XMM-Newton satellite  
 278 were fabricated there. However, many applications demanded large detectors which would  
 279 not fit on a 4-inch wafer. In addition environmental constraints motivated a move of the  
 280 lab to Neuperlach. There we found perfect conditions on the Siemens Campus: 1000  $m^2$   
 281 cleanroom, with 600  $m^2$  of class 1 (Fig. 5).

282 In addition the lab profited from the production facilities of Siemens supporting the main-  
 283 tenance of our cleanrooms and offering services like ion implantation and waste water  
 284 processing. The lab was now equipped for 6 inch wafers which allowed to engage in the  
 285 development of detectors for ATLAS SCT, ILC, Belle II and other projects. A strength  
 286 of the lab were 3D-simulations of silicon detectors which allowed us to design the electric  
 287 fields in the silicon bulk, optimizing drift and charge collection properties. The laboratory  
 288 got also more and more involved in the development and fabrication of sensors for other  
 289 institutes of the Max-Planck-Society. This was one reason that the organisation of the lab-  
 290 oratory was changed in 2013. It became an independent entity of the Max-Planck-Society.  
 291 Still it maintains close connections to the MPP.

### 292 3.3 Silicon Tracker: ATLAS

293 Originally silicon detectors were exclusively used for vertexing where it is sufficient to  
 294 measure the track direction close to the interaction point. Therefore these detectors can  
 295 be small and need only few silicon sensors. This is different for tracking detectors where





Figure 5: Part of the class 1 cleanroom of the HLL in Neuperlach (2000 -2024)

296 good momentum resolution requires a long lever arm and several measurements along  
297 the track trajectory. Consequently these detector need to be large which excluded silicon  
298 detectors for cost reasons. However, in high rate environments, like at the LHC, gaseous  
299 detectors cannot be used because of occupancy and radiation damage. Silicon detectors,  
300 however, can still be operated under such conditions. Fortunately, the superior resolution  
301 of silicon detectors makes allows to achieve the same momentum resolution with a more  
302 compact device, leading to an overall reduction of the detector system (magnetic coil,  
303 calorimeters) with considerable cost savings balancing in part the higher costs of a silicon  
304 tracker. ATLAS [39] is a detector which has to operate in this extremely harsh radiation  
305 environment. This introduces new challenges which were unknown at the experiments  
306 preformed so far. The intense radiation will change the effective doping of the silicon  
307 sensors beyond type inversion, hence provisions have to be made that the sensors still  
308 operate with reasonable performance. Cost considerations lead to the choice of rather  
309 standard single sided strip sensors with p-strips in n-type bulk [14]. In order to reach full  
310 charge collection efficiency after  $10^{13}$  neutrons/cm<sup>2</sup> these sensors need to be biased with  
311 voltages of 400V. Multiple guardrings and other layout features ensure stable operation  
312 at this high voltage. The sensors have to be cooled ( $< -7^{\circ}\text{C}$ ) for two reasons:

- 313 • Reverse annealing which would eventually increase the depletion voltage beyond  
314 400 V is reduced at that low temperature.
- 315 • High leakage currents together with the high operation voltage could lead to self-  
316 heating of the sensors which by positive feedback can result in thermal runaway. By  
317 cooling leakage currents must be kept below a critical value.

318 ATLAS SCT uses binary readout. The readout chip has a programmable threshold, only

319 hits passing this threshold are read out. This simplifies the readout system and reduces  
 320 the bandwidth. The noise of the system is about 1500 electrons (ENC). With this noise  
 321 the threshold can be set to achieve a noise occupancy of  $10^{-5}$  at a hit efficiency exceeding  
 322 95%. The ASIC is produced in a radiation hard DMILL BiCMOS process [15]. The sensors  
 323 [14] are single sided, two of them are joined together with the strips along the z-direction  
 324 connected. Another such pair is positioned back to back with 40 mrad angle to achieve  
 325 stereo information. The electronic hybrid is either attached to the module end (endcap  
 326 modules) or bridged across the sensors (barrel modules). These modules are arranged in  
 327 four barrels (1.5 m long at radii of 28 cm, 36 cm, 43 cm, and 50 cm) and two times nine  
 328 discs in the forward regions, extending up to  $z = \pm 2.7$  m. The complete detector consists  
 329 out of almost 20000 silicon sensors. The 10000 sensors in the barrel region are rectangular.  
 330 Three differently shaped wedge type sensors are used in the forward discs. The total area  
 331 covered is  $60 \text{ m}^2$  with  $7 \times 10^6$  readout channels. This should be compared to the ALEPH  
 332 detector which had 96 detectors,  $0.25 \text{ m}^2$  with 70.000 readout channels.  
 333 As mentioned above the low temperature operation requires an efficient cooling system  
 334 which should still have low mass. ATLAS uses evaporative cooling: liquid  $\text{C}_3\text{F}_8$  is evapo-  
 335 rated in the cooling pipes situated in the module support structure. The temperature is  
 336 regulated by setting the pressure in these pipes. The heat transport from the sensors and  
 337 electronics to the cooling contact is made using materials with very high thermal conduc-  
 338 tivity like carbon-carbon and thermal pyrolytic graphite. To avoid heating of the sensors  
 339 by the electronics the heat path of both is separated as much as possible. The system is  
 340 able to remove about 50 kW of power keeping the sensors at a temperature of  $-7^\circ\text{C}$ .

341 The specifications of the ATLAS strip detector is shown in Table ?? .



Figure 6: A module of the ATLAS SCT forward disks

342 MPP was heavily involved in the design and construction of the forward disks. The  
 343 mechanical desing of the modules and the use and optimization of the heat spreaders made  
 344 from pyrolitic graphite was done in the technical department. The HLL played a leading  
 345 role in the design of the silicon sensors, proposing the use of n-in-n detectors. Clearly  
 346 the capacity of the HLL was not sufficient to produce the large amount of sensors needed  
 347 for the SCT. However, the production of prototype test sensors allowed to test various  
 348 design options before the final design was chosen. MPP proposed a novel way of biasing  
 349 the detectors using implanted resistors instead of the conventional polysilicon resistors.

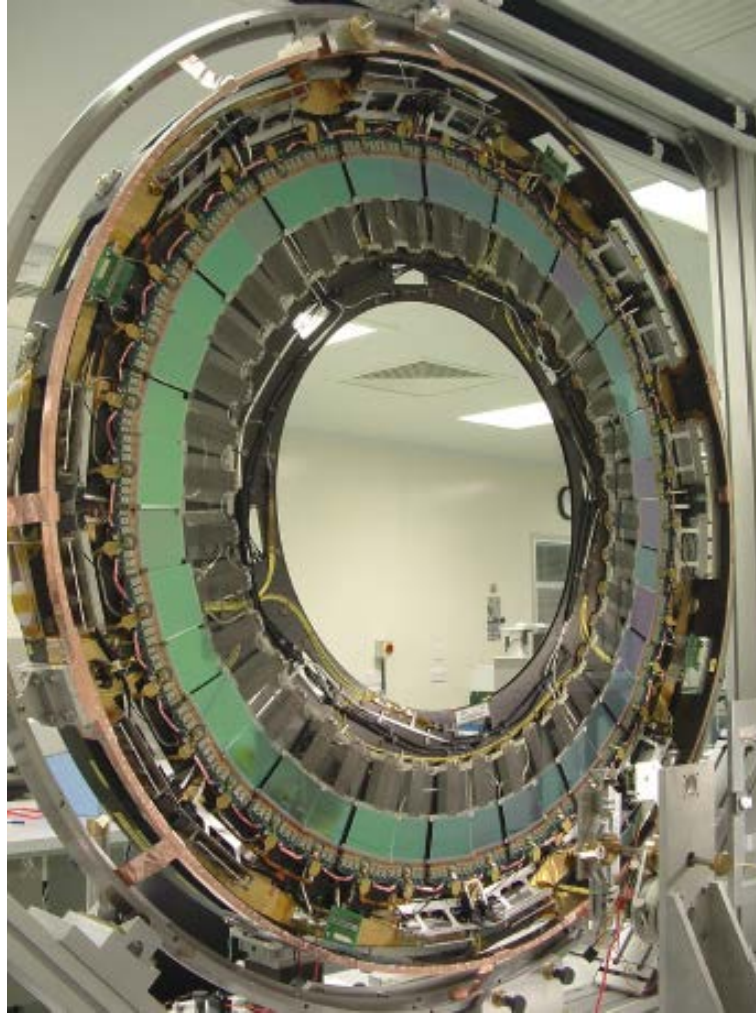


Figure 7: One of the ATLAS SCT forward disk with short middle modules assembled at MPP.

350 This simplified the production process and reduced the costs, not unimportant for the  
351 large scale production required. With CIS in Erfurt MPP found a company which could  
352 fabricate the detectors according to our specifications. A fraction of the detectors for the  
353 forward discs were fabricated by CIS, shipped to the HLL and tested there. The second  
354 manufacturer was Hamamatsu producing detectors with similar specifications. Then the  
355 detectors were distributed to the various assembly sites where the SCT modules were  
356 assembled. MPP itself assembled 420 modules for the inner forward rings. Figure 6 shows  
357 a forward module produced at MPP and Fig. 7 one of the forward rings equipped with  
358 such modules.

359 The detector started operation in 2011 and is still performing as specified.

360 *Anything about ATLAS pixel?* Even more challenging is the innermost region of the  
361 ATLAS detector where the pixel vertex detector is located. Especially after the high lu-

362 minosity upgrade of LHC the radiation damage becomes so severe that standard detectors  
363 cannot work anymore. New concepts had to be developed, like thinned n-in-n detectors.  
364 Here the MPP contributed together with the HLL to the development of such detectors.

### 365 3.4 DEPFET Pixel Detectors: Belle II

366 At extremely high luminosities the track densities and therefore the detector occupancies  
367 in double sided (or any projective) silicon detectors become to large and the ambiguities  
368 cannot be resolved any more. Here pixel detectors are needed. A simple diode array  
369 detector is rather easy to produce, but the difficulty lies in the readout of thousands of  
370 individual pixel. ASIC chips can do the job, but they have to be directly mounted on  
371 top of the silicon sensor, besides the challenging small pitch connection technology which  
372 introduces a challenge the amount of material per sensors the material budget increases  
373 considerably. This is a minor problem for LHC detectors like ATLAS: the particles have  
374 high momenta with low multiple scattering. However, if tracks of lower momenta (in the  
375 GeV/c regime) need to be reconstructed with high precision very thin detectors are needed  
376 and the hybrid concept with the detector-readout sandwich concept fails.

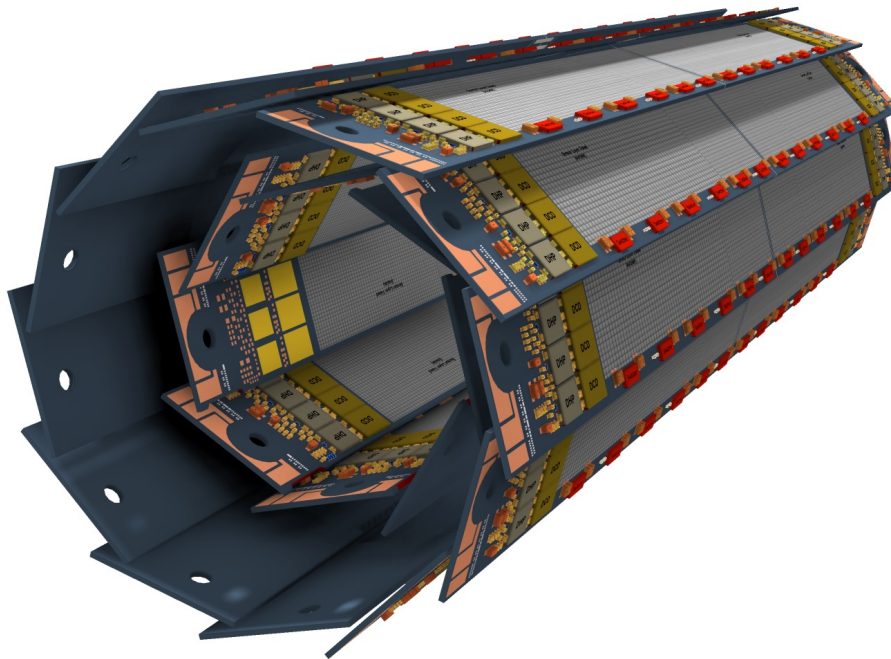


Figure 8: Artist's view of the ladder arrangement of the Belle II PXD. Two modules are glued to form ladders which are arranged cylindrically around the beam pipe in two layers at radii of 1.4 cm and 2.2 cm, the length is 17 cm.

377 At the HLL we developed a concept of a monolithic silicon pixel detector with an integrated  
378 first amplification stage. The amplified signal can then be routed to the readout electronics  
379 outside the sensitive area of the device using a rolling shutter scheme. This detector, called



380 DEPFET (**D**epleted **p**-channel **F**ield **E**ffect **T**ransistor) [16, 17] was originally developed  
381 for an experiment at the future ILC collider, but found its first application in the Belle II  
382 experiment. Belle II is an upgrade of the original Belle experiment (1999-2010), intended  
383 to operate at a 40 times higher instantaneous luminosity. This high luminosity drastically  
384 increases the occupancy which makes it impossible to use double sided silicon detectors, as  
385 in Belle, for the inner layers of the vertex detector. This was a real problem since precise  
386 vertexing is absolutely necessary for the measurement of CP-violation, one of the main  
387 motivations of Belle II. The DEPFET detectors which, due to their high signal to noise  
388 ratio, can be produced with a sensor thickness as low as  $50\mu m$ , using a novel technology  
389 based on wafer bonding (in the final detector a more conservative  $75\mu m$  were used to have  
390 a higher S/N allowing to compensate radiation damage). The detector, shown in Figures  
391 8 and 9 consists of two layers with DEPFET modules.

392 Because of the all-silicon concept (no extra material as carrier needed) and the possibility  
393 to place most of the electronics outside the acceptance a material length of only  $0.21\%$   
394  $X_0$  per layer could be achieved. The detector can be compared with a CMOS camera of 6  
395 megapixel producing 50.000 images a second. No other detector concept available at that  
396 time (2008) was able to achieve this. When we proposed this to the Belle II collaboration  
397 this was immediately accepted and MPP became member of Belle II. This project was  
398 exactly the kind of project the HLL was made for: a high performance detector with a  
399 novel, sophisticated technology which cannot be produced by industrial partners but still  
400 small enough not to exceed the production capacity of the HLL.

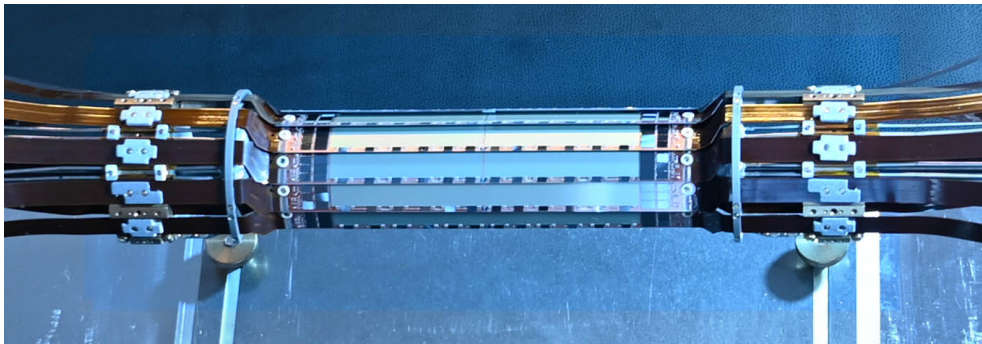


Figure 9: The Belle II PXD after assembly at MPP. The detector has 8 detector elements in the inner layer and 12 in the outer (here visible).

401 It took a long time to construct the detector, especially the handling of the ultra thin  
402 and therefore fragile sensors posed many challenges. Despite all difficulties we managed to  
403 install a first version of the detector (with only one of the originally foreseen two layers)  
404 right in time for the first physics run in 2019.

405 With the luminosity collected until 2022 many physics analyses were done demonstrating  
406 the excellent performance of this detector. As expected the vertex resolution improved  
407 by a factor of two compared to the predecessors Belle and BaBar, as shown in Fig. 10.  
408 Notable are the most precise measurements of the lifetimes of D-Mesons [18, 19] and  
409 Baryons [20, 21], with a precision improved by a factor of 200 compared to the ACCMOR

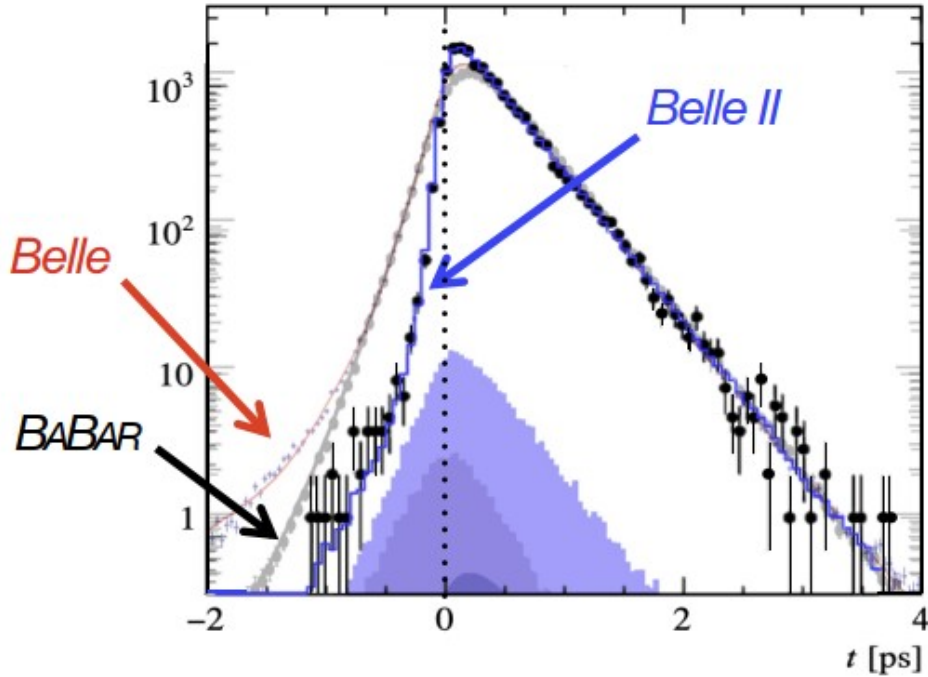


Figure 10: Decay times of  $D^0$ -Mesons: the negative tail is a measure of the lifetime resolution which is about a factor of two better at Belle II compared to Belle and BaBar.

410 measurements four decades earlier. In the shutdown from 2022-2023 a new detector with  
 411 the second layer completed, was installed and is taking data now. Even today it is still  
 412 the thinnest vertex detector in a running experiment.

413 Apart from the unique pixel vertex detector PXD the Belle II detector houses another  
 414 unique system, also concerned with charged particles, namely a track trigger at the  
 415 deadtime-free first level, which is based on neural networks. In Belle II two main trigger  
 416 systems are installed, namely the calorimeter trigger, derived from the electromagnetic  
 417 Cs(Tl) calorimeter, and the track trigger, using the sense wires from the Central Drift  
 418 Chamber (CDC). The standard track trigger of Belle II was designed to find tracks in  
 419 the plane transverse to the beam direction (“2D tracks”), using only the axial wires of  
 420 the CDC. A major problem for this track trigger are charged particles originating along  
 421 the beam (“z”) direction far from the interaction point (IP) of the colliding electron and  
 422 positron beams.

423 It was recognized early by the Belle II group at the Institute that a track trigger needs  
 424 to be developed which could recognize and reject the dominating rate from the off-Z  
 425 interactions. While traditional track fits at the first trigger level would exceed by far the  
 426 allowed latency, the massively parallel computation power of neural networks and their  
 427 ability to adapt to changing background conditions were chosen to provide a robust first  
 428 level “z” trigger. The networks use as input the results from the standard Belle II 2D

429 trigger and add the stereo wire information to provide estimates for the origin of the 2D  
430 track candidates in direction of the colliding beams (“ $z$ -vertex”), as well as their polar  
431 emission angles  $\theta$ . Given the  $z$ -vertices of the “neural” tracks allows suppressing the  
432 overwhelming background from outside by a suitable cut  $d$ . Requiring  $|z| < d$  for at least  
433 one neural track in an event with two or more 2D input candidates will set an L1 track  
434 trigger. The networks also enable a minimum bias trigger, requiring a single 2D track  
435 candidate validated by a neural track with a suitable momentum cut in addition to the  
436  $|z|$  condition. Both the preprocessing of the input variables and the neural computations  
437 are implemented on FPGAs with a latency of only 300 ns [22]. The neural trigger is  
438 successfully running in Belle II since the year 2020 and has fully replaced the standard 2D  
439 track trigger of Belle II.

440 The hardware level neural network track trigger of the Belle II experiment represents a  
441 significant step towards fast and intelligent data collection and processing methodologies  
442 in scientific research. The innovative approach to integrate machine learning techniques  
443 into the hardware of the experiment indicates the possibility for a paradigm shift towards  
444 embracing smarter and faster solutions for real-time event selection. It also sets a precedent  
445 for future experiments where efficient and accurate data collection as well as extraction of  
446 novel features are essential.

## 447 4 Calorimetry in High Energy Physics

448 In high energy physics experiments calorimetry is a standard procedure to measure the  
449 total energy of particles. Particles impacting the calorimeter detector lose via secondary  
450 interactions with the absorber material all their energy. Here sampling calorimeters have  
451 alternating layers of passive absorber material and active layers, where the deposited en-  
452 ergy is measured. When a secondary charged particle passes the liquid argon (LAr) gap,  
453 it takes about 23.6 eV to ionize an electron. Applying high voltage at the electrode of the  
454 gap, electrons (fast) and ions (slow) drift to the anode resp. cathode. This signal is am-  
455 plified and recorded and the total integral of these signals is proportional to the impacting  
456 particle energy  $E$ . With increasing energy the precision of this measurement is increasing  
457 and therefore calorimetry is gaining more and more importance at high energies. With  
458 rising particle energies  $E$  the energy resolution is improving as  $\sim 1/E^{1/2}$ . Calorimeters  
459 are sensitive to charged as well as to neutral particles and the depth of a calorimeter re-  
460 quired to absorb all the energy is increasing only logarithmically with energy. Optimizing  
461 the lateral segmentation the impact angle of a particle can be measured precisely. The  
462 longitudinal segmentation allows to study the shower shape of the impacting particle and  
463 thus enables an effective particle identification. A fine segmentation - laterally as well as  
464 longitudinally - is crucial when combining track measurements with clusters reconstructed  
465 in the calorimeter. Calorimeters are fast detectors and are thus well matched to high  
466 luminosity colliders. As quarks fragment into many particles, the jet energy measured at  
467 high energies can be directly correlated with the parton energy. With a fine segmented  
468 preshower layer an energy correction for inactive material in front of the calorimeter can be  
469 obtained, as well as an effective  $\gamma/\pi^0$  separation. These features yield strong arguments  
470 for calorimetry at high energy colliders and make the calorimeter an essential part of the

471 detector. In the case of liquid argon calorimeters, where the active layer is a liquid argon  
472 gap sandwiched between high voltage electrodes, additional arguments like radiation  
473 hardness and signal stability play a key role.

#### 474 4.1 CELLO - Start of the Liquid Argon Calorimetry at the Institute

475 The CELLO experiment [23] at the  $e^+e^-$  storage ring at DESY with the spokesperson H.  
476 Oberlack started 1979. Mainly French and German institutions joined in a combined effort  
477 to study  $e^+e^-$  interactions at 34 GeV, later increasing up to 47 GeV center of mass energy.  
478 The main focus at PETRA was the search for the - at that time - unknown top quark,  $\tau$  -  
479 decays and QCD studies ( $\alpha_s$  measurement). Jet studies were thus at the 'gluon discovery  
480 machine' an important issue. These goals defined the requirements for the calorimetry  
481 at CELLO: very good energy resolution for electrons and photons, good electron/hadron  
482 separation, good jet reconstruction and muon identification. The excellent  $\pi^0$ ,  $\gamma$  and jet  
483 reconstruction of the calorimeter were the basis for the success.

484 The liquid argon calorimeter (LAr) was the optimal choice for the requirements of the  
485  $e^+e^-$  physics at PETRA.

486 The long term stability of the calibration is minimizing any systematics. This holds even  
487 for a very harsh environment situation. A high flexibility with respect to lateral and  
488 longitudinal segmentation is an important feature. It offers the chance for an optimiza-  
489 tion of the energy and spatial resolution as well as an effective electron/hadron resp.  
490 hadron/muon separation. With a fine segmented preshower layer an energy correction  
491 for inactive material in front of the calorimeter can be obtained, as well as an effective  $\gamma$   
492  $/\pi^0$  separation. The Fig.11 shows the schematic view of the CELLO detector. The re-  
493 sponsibilities for the Pb/LAr calorimeter were the institute (barrel) and Orsay (endcap),  
494 for the tracking detector the institute (drift chamber) and Orsay (proportional chamber)  
495 and for the muon chambers Saclay. One of the outstanding features was the thin coil  
496 ( $0.49 X_0$ ) of the superconducting magnet (1.3 T), thus minimizing any energy losses in  
497 front of the calorimeter. The total number of the calorimeter read-out channels was 6880,  
498 the total weight of the detector was 1400 t. The calorimeter group of the institute was  
499 responsible for the construction of the  $2 \times 8$  barrel modules, the barrel cryostat with all  
500 16 feed-through's, the read-out electronics, the calorimeter trigger, the data acquisition  
501 and the reconstruction software. Pb-strips of 1.2 mm thickness and 2.3 cm width with 3  
502 orientations and 3.6 mm thick LAr gaps were the basic structure. The total thickness of  
503 one module was  $20 X_0$  with a 6-fold sampling in depth.

504 Obviously the start of such a project was very challenging for the institute, in particular  
505 also for the technical department. The know-how of cryogenic systems had to be devel-  
506 oped in house - in collaboration with the Kernforschungszentrum Karlsruhe, with major  
507 requirements on quality control. It was a major challenge to get all seals (cover and feed-  
508 through's) tight in the cold in view of the mechanical strains and stresses due to the load  
509 and temperature gradients. Because of lacking funds, in the first phase the number of  
510 read-out channels was reduced with a special cabling scheme. Therefore a reopening of  
511 the cryostat with finalizing the originally planned read-out granularity was required. In



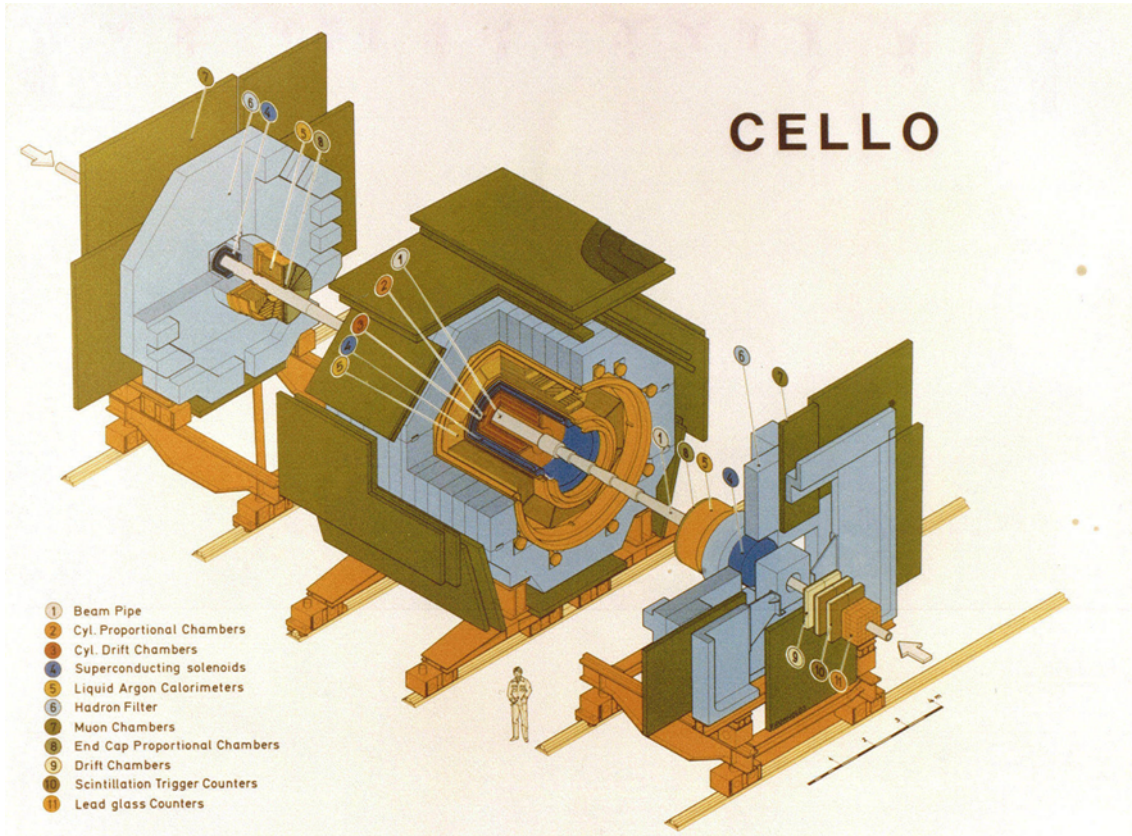


Figure 11: Schematic view of the CELLO detector. Shown are the main detector components: the drift and the proportional chambers of the tracker(2,3), the superconducting magnet(4), the Pb-LAr calorimeter(5), the hadron filter(6) to stop all particles except the muons, and the muon chambers(7).

512 consequence, welding the cover of the cryostat, as usually done nowadays, was not a valid  
 513 option. Finally a coil spring coated with PTFE was the optimal solution rather than the  
 514 usual Indium sealing technique used at that time. Just to give an example, prior to the  
 515 shipment to DESY the final cryostat has been cold tested in a special construction hall  
 516 nearby rented by the institute. Also the module construction has been studied in special  
 517 *R&D* tests at CERN to verify the performance for electrons:  $\sigma/E = 8.5\%/E^{1/2}$  for the  
 518 energy resolution and typically 4 mrad for the angular resolution. Finally the Fig.12 shows  
 519 the insertion of one barrel module in the cryostat of the CELLO detector at DESY.

520 At PETRA detailed studies of the gluon - with the typical three jet structure in hadronic  
 521 events - was one of the primary goals. In consequence, high precision  $\alpha_s$  determination  
 522 was a challenging goal for all PETRA experiments. CELLO focused in particular on the  
 523 systematic issues of the various methods used, as analysis based on thrust, jet masses,  
 524 energy-energy correlations or total cross section [38].

525 Among the many physics highlights of the CELLO experiment, one particular analysis  
 526 should be mentioned here, which took full advantage of the high granularity of its LAr

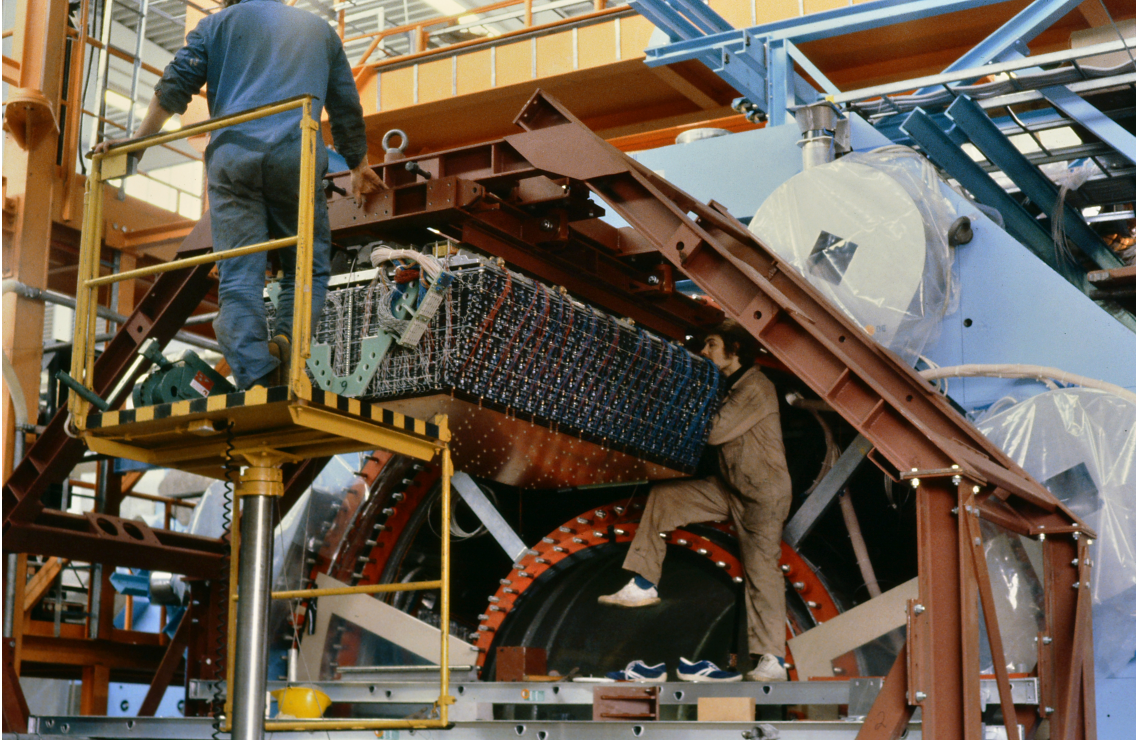


Figure 12: Insertion of one barrel calorimeter module in the cryostat of the CELLO detector at DESY.

527 calorimeter. With the Cello calorimeter it was possible to solve a long-standing puzzle in  
528 the decay branching ratios of the tau lepton. The puzzle was coined as the “1-Prong Prob-  
529 lem”: The branching ratio of the tau leptons decaying into 1 charged particles plus neutrals  
530 (neutrinos and neutral hadrons) was found too small relative to the branching ratio into  
531 3 charged particles plus neutrals. Using the new and highly efficient LAr calorimeter the  
532 “missing” neutral particles to contribute to the 1-prong decays were identified as neu-  
533 tral pions, decaying into two photons. A new analysis method using a transition matrix  
534 technique finally established the tau lepton with branching ratios and other properties as  
535 expected by the Standard Model [24]. The results of the CELLO experiment was later  
536 verified by the experiments at LEP, notably by ALEPH.

## 537 4.2 H1 - Hadronic Calorimetry and Software Compensation

538 In 1986 the H1 collaboration started with the construction of the detector (see Fig.13) [25]  
539 at the electron proton collider HERA at DESY. The highly asymmetric energies of the  
540 electron (27.5 GeV) and proton (820 - 920 GeV) asked for an asymmetric detector [25] -  
541 and calorimeter [26] - with special emphasis on the high energy forward (proton) region.  
542 The size of the detector was  $12 \times 15 \times 10$  m, the total weight 2800 t. The total number of  
543 calorimeter read-out channels was 44352. The study of the proton structure functions, i.e.  
544 quark and gluon parton distributions, was one of the primary goals. This is an essential

545 input in pp physics to understand the basic standard model cross sections and thus be  
546 able to pin down any deviations pointing to new physics beyond the standard model. The  
547 phase space covered for the study of proton structure functions had to be as large as  
548 possible. Together with the study of neutral ( $\gamma, Z$  exchange) and charged (W exchange)  
549 electroweak currents this yields severe constraints on the calorimeter performance. This  
550 holds also for the QCD studies and  $\alpha_s$  determination.

551 The H1 LAr calorimeter (2.4 mm argon gap, see Fig.14) is positioned within a supercon-  
552 ducting solenoid to minimize any inactive material in front of the calorimeter.

553 To match the physics requirements a special optimization of the cracks between the indi-  
554 vidual modules was necessary (see Fig.15): for neutral current events, where the electron  
555 has to be reconstructed with high precision, pointing  $\phi$  cracks have been chosen. The  
556 losses are minimized and excluding the bad crack regions the reconstruction is optimal.  
557 For charged current events the missing energy has to be reconstructed well, eliminating  
558 the option of fiducial volume cuts. Therefore the hadronic calorimeter is designed with  
559 non-pointing  $\phi$  cracks, eventhough the worsening of energy reconstruction in a larger ac-  
560 ceptance region is the consequence.

561 The absorber material of the electromagnetic calorimeter is Pb with a thickness of 2.4 mm,  
562 sandwiched between two thin fiberglass plates glued to them. The institute was responsi-  
563 ble for the forward hadronic calorimeter (FB1, FB2, OF1, OF2) wheels (see Fig.14). The  
564 hadronic calorimeter is made of stainless steel (thickness 16 mm) as absorber. The toler-  
565 ances on thickness and flatness for plates of this size do not allow to define the LAr gap  
566 with the required precision. Therefore high precision read-out cells are inserted between  
567 the absorber plates. Two outer stainless steel plates define the independent read-out board  
568 with a LAr double gap and a G10 read-out structure board in the center. Polyimid films  
569 are glued to the stainless steel plates and covered with a high resistive coating for the HV  
570 distribution. Thus an effective spatial resolution is obtained without the need for a fine HV  
571 pad structure connected via large resistors to HV. In addition, this technique guarantees  
572 an optimal HV protection for the read-out amplifiers. Because polyimid films with high  
573 resistive coating were at that time not available, the printing of this high resistive layer  
574 has been developed in the institute. With the strong requirements on components, drying  
575 and bake-out time the printing procedure was done in house. The company in charge  
576 did the printing with the quality control by local staff. In a rather unconventional way, the  
577 printing machine was given to the company at the end of the construction as part of the  
578 payment. Only thus the required precision of a touchy production step could have been  
579 guaranteed.

580 As the steel-LAr calorimeter is non-compensating, a special signal weighting approach  
581 has been developed in close collaboration with DESY: the software-compensation. Signals  
582 are calibrated according to the signal density which distinguishes hadronic from electro-  
583 magnetic showers. Detailed beam tests were done at CERN to optimize the detector  
584 granularity for this weighting approach, as well as to test the module performance and  
585 quality. Finally for different impact angles the calorimeter has been calibrated in dedi-  
586 cated beam runs at CERN. The physics requirements of an energy resolution for electrons  
587 of  $\sigma/E = 12\%/E^{1/2}$  and for the hadrons (with weighting) of  $\sigma/E = 45\%/E^{1/2} \oplus 1\%$  have

588 been achieved.

589 The H1 LAr calorimeter was also equipped with a very efficient and low-energy threshold  
590 trigger at the first level, based on special electronics designed and built by the Institute's  
591 electronics department. As a key feature the LAr trigger was finding individual isolated  
592 clusters over almost  $4\pi$  acceptance. The clusters had a transverse dimension of approx-  
593 imately the size of typical jets at HERA energies, therefore named "Jet Trigger". Each  
594 cluster yielded the deposited energy and its polar and azimuth emission angles. With the  
595 Jet Trigger, in combination with the track information from the central drift chamber it  
596 was, for example, possible to measure the longitudinal structure function of the proton  
597 in a completely new kinematic regime [27]. Another highlight from the H1 experiment  
598 was the first realization in a HEP experiment of a neural network trigger, trained with  
599 real data for specifically selected final states. The basic unit of the neural trigger was  
600 a commercial neuromorphic chip integrated on a VME board. This hardware was still  
601 pretty slow compared to modern FPGAs, with an execution time of 20  $\mu$ s. It was there-  
602 fore deployed on the second trigger level ("L2") of the 4-level H1 trigger system. The  
603 neural trigger used the information from the main subdetectors of H1, combine them and  
604 do a pattern recognition of physically interesting final states. For an efficient triggering of  
605 the desired final states, the conditions of the respective L1 triggers were relaxed and the  
606 extra L1 trigger rate, caused by other "background" physics channels, was reduced by the  
607 networks to an acceptable level [28].

608 One of the physical highlight of the neural trigger was the measurement of the cross  
609 section for exclusive elastic production of  $J/\psi$  mesons as function of the total photon-  
610 proton center of mass energy. The H1 result [29] showed a strong increase of the cross  
611 section towards large center of mass energies. This result was in disagreement with Regge  
612 theory, postulating Pomeron exchange with an almost energy-independent cross section.  
613 Later, new predictions based on QCD calculations were found to be in agreement with  
614 the H1 measurement.

615 The Fig.16 shows the first hadronic calorimeter module built in the institute with the H1  
616 calorimeter project leader H. Oberlack.



# HERA Experiment H1

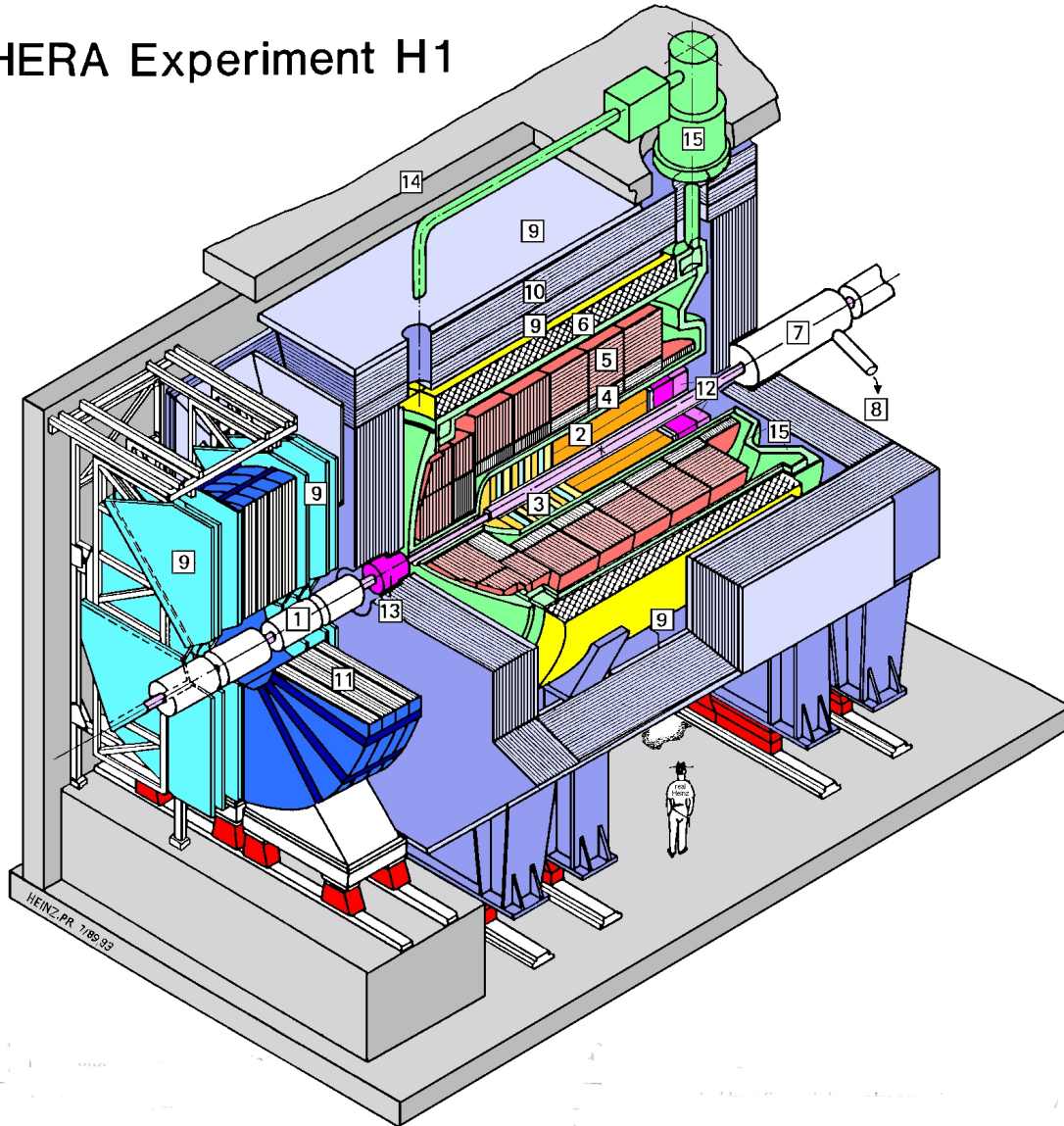


Figure 13: Layout of the H1 detector at HERA. The electromagnetic(4) and hadronic(5) LAr calorimeters are just next to the central tracker(2) and within the superconducting coil(6). The muons are measured in the muon chambers(9).

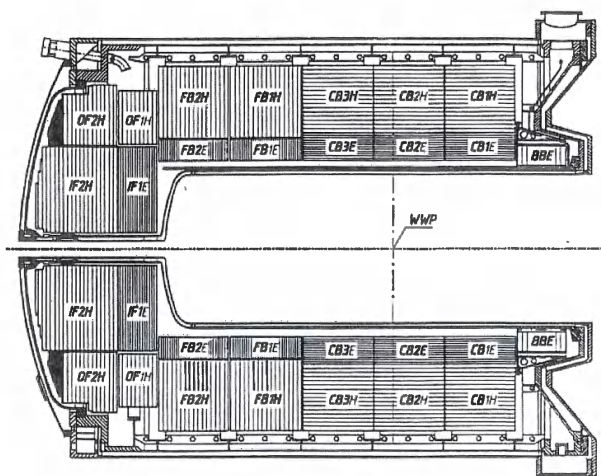


Figure 14: The r-z view of the H1 LAr calorimeter. Shown are the electromagnetic and hadronic sections of the LAr calorimeter. The high energy protons are entering from the right, the electrons from the left. The asymmetry in the energies defines the geometry of the set-up.

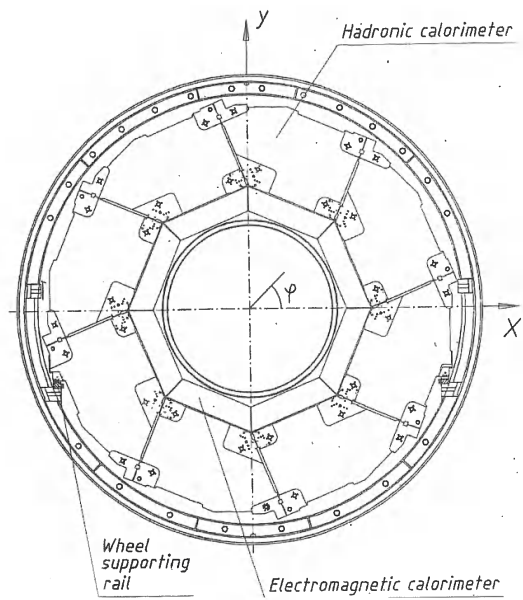


Figure 15: The  $r - \phi$  view of the H1 LAr calorimeter. The  $\phi$  cracks are pointing to the interaction point for the electromagnetic sections and non-pointing for the hadronic sections.

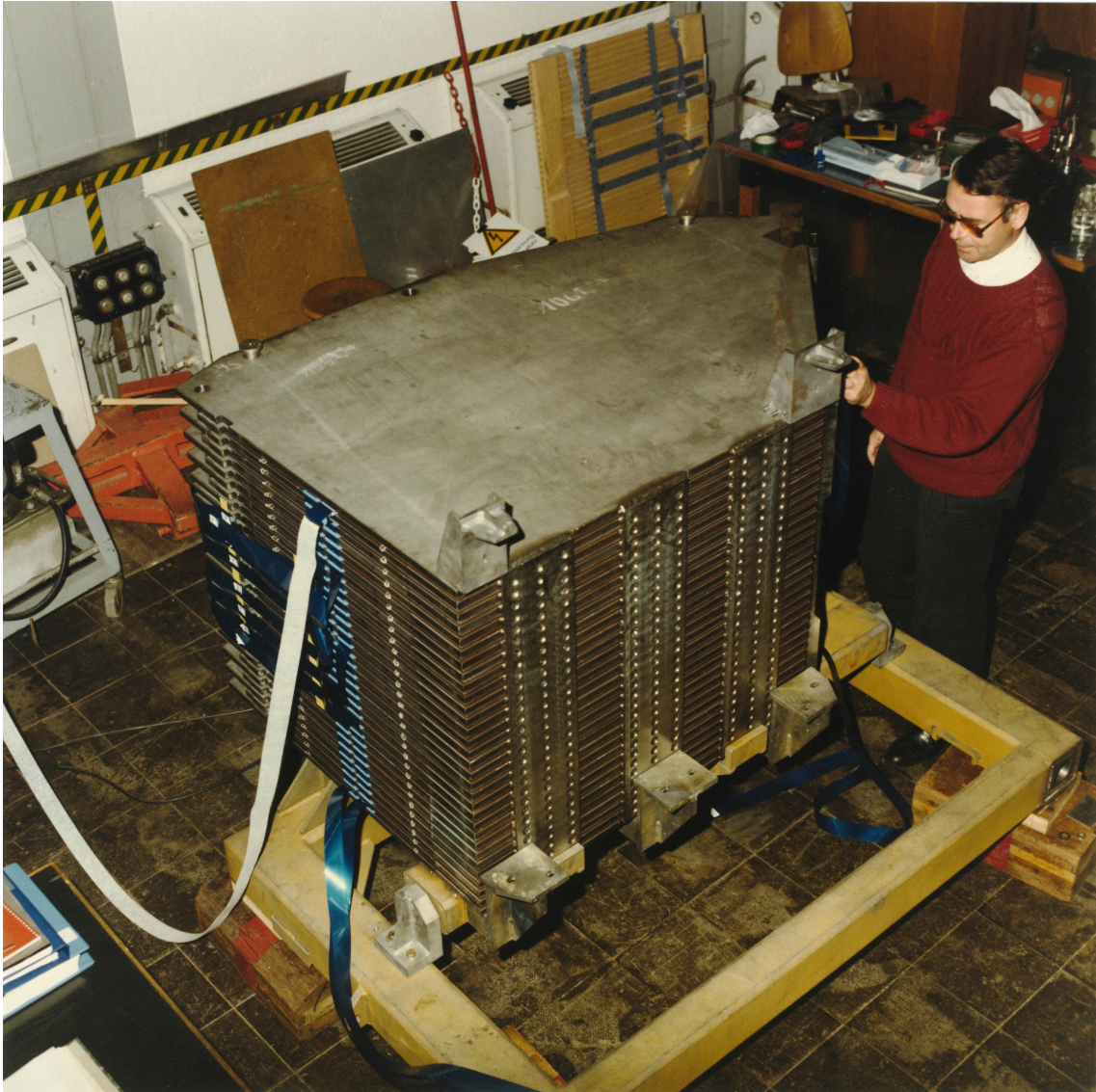


Figure 16: The first hadronic calorimeter module of the H1 calorimeter with the H1 calorimeter project leader H. Oberlack.



617 **From ASCOT to ATLAS: the Route to the LHC**

618 In 1990 started the preparation for the design of a detector at the pp storage ring LHC.  
619 The high luminosity with an unprecedented number of interactions per collision imposed  
620 a challenge for an optimal detector concept at that times. The muon reconstruction  
621 and trigger were therefore the first priority. The solution was an aircore toroid mag-  
622 net with muon drift tubes. Next in priority was a good reconstruction of electrons and  
623 gammas, with the benchmark process of the Higgs boson decay  $H \rightarrow \gamma\gamma$  in mind. The  
624 goal was an energy resolution for  $\gamma$ 's of  $\sigma/E = 9.5\%/E^{1/2} \oplus 0.5\%$  and an for hadrons of  
625  $\sigma/E = 50\%/E^{1/2} \oplus 2\%$  (with energy weighting). In close collaboration with the Ruther-  
626 ford lab the institute presented an expression of interest - ASCOT [30] (Apparatus with  
627 SuperCONducting Toroids) - in 1992 at the CERN meeting in Evian. The spokesperson  
628 of the ASCOT collaboration was F.Dydak. The Fig.17 shows the schematic view of the  
629 detector.

630 For the LAr calorimeter small LAr gaps were proposed, to limit the charge collection time.  
631 As the drift time for ions is typically a factor of 1000 larger than for electrons, at very  
632 high luminosities the electric field in the LAr gap is severely distorted. Thus in view of the  
633 high luminosity a small LAr gap also guarantees to stay away from the critical ionization  
634 density in the forward region. Vice versa, small gaps increase the capacity, thus increasing  
635 the noise and worsening the signal to noise ratio. Therefore the concept of 'active pads'  
636 has been proposed: each signal from an individual pad is fed via preamplifiers in the cold  
637 to a summing stage (also in the cryostat). Thus the ganging in depth is done fully in cold.  
638 The development of cold electronics has been started in the calorimeter group already in  
639 1990 and finalized in the RD33 test at CERN [32]. A second important aspect was the  
640 minimization of systematics. Keeping the impact angle relative to the absorber orientation  
641 almost constant within the full rapidity  $\eta$ -range the sampling ratio is almost constant and  
642 any losses due to cracks in  $r - z$  can be avoided. With an impact angle of  $45^\circ$  this has been  
643 realized in the 'Thin Gap Turbine' (TGT) [31] in the  $\eta$ -region  $|\eta| \leq 5.0$ . The Fig.18 shows  
644 the TGT layout of the proposed ASCOT calorimeter in  $r - z$ . The size of the individual  
645 read-out boards is chosen to be rather small to be able to keep also the cracks in  $\phi$  at  
646 a minimum. Three LAr double gaps, each 0.4 mm wide, two PB plates (1.6 mm thick)  
647 covered with thin stainless steel, three G10 read-out boards covered with high resistive  
648 polyimid and two outer stainless steel plates (2.0 mm thick) yield the basic read-out board  
649 unit. The cold preamplifiers are in small cutouts of the outer stainless steel plate. The  
650 pad signals are then routed to cold summing boards located at the outer periphery of the  
651 calorimeter. This concept has been tested with a calorimeter with 36 independent readout  
652 boards at CERN [32] and the requirements for the LHC were fulfilled.

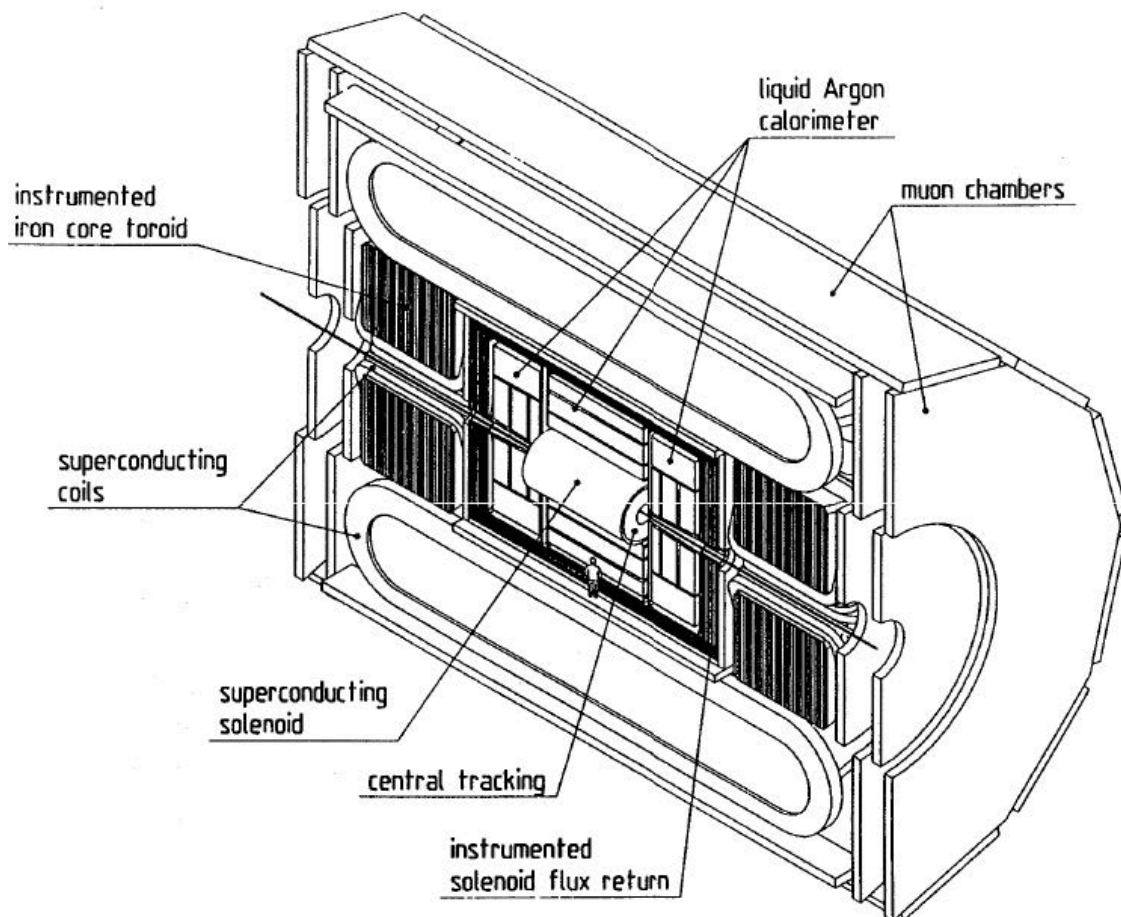


Figure 17: Schematic view of the proposed ASCOT detector layout. Shown is the superconducting solenoid with the tracking detector, the LAr calorimeter and the superconducting toroid coils with the muon chambers.

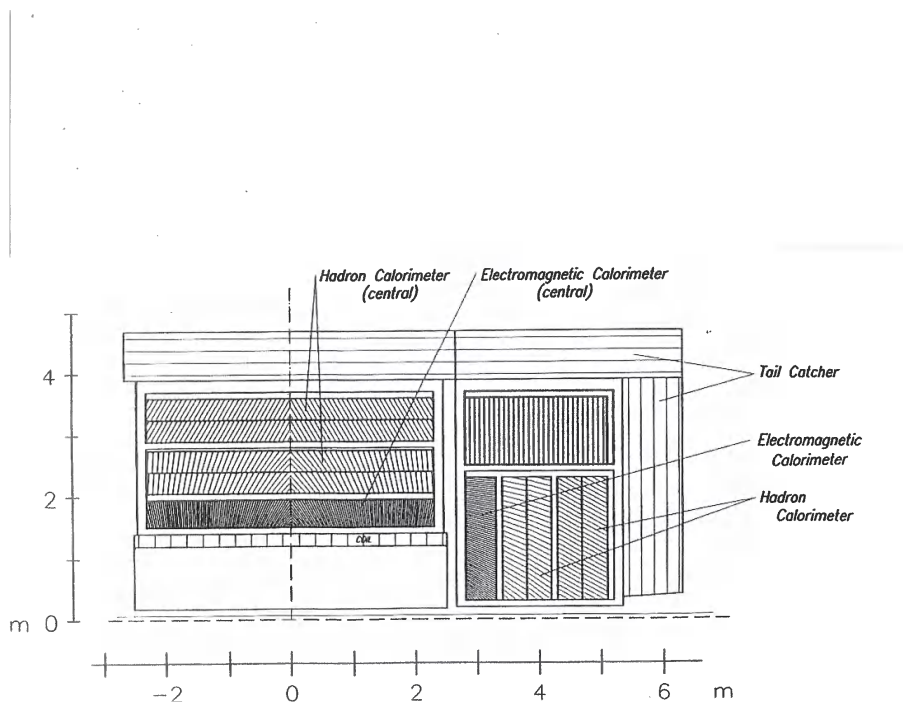


Figure 18: The r-z view of the proposed LAr calorimeter for the ASCOT detector. The absorber plate orientation is chosen to be at a constant angle of  $45^\circ$  relative to the particle impact direction for the full range in  $z$  of the detector.

653 Following the Evian meeting CERN decided to support only two general purpose detectors  
654 at the LHC. Thus the collaboration had to merge with interested partners. A similar  
655 approach (LAr) for the calorimetry was proposed by the EAGLE collaboration, eventhough  
656 a warm Fe toroid has been chosen for the muon spectrometer. Both collaborations started  
657 discussions how to converge to one detector - the start of the ATLAS detector. In October  
658 1992 the letter of intent [35] has been presented. For the muon spectrometer the aircore  
659 toroid has been kept, for the LAr calorimeter both options, the accordeon [33] and the  
660 TGT [34] have been kept. The final decision was planned to be taken at the ATLAS  
661 proposal [36].

662 Soon after a period of very intense discussions of various subgroups started in the ATLAS  
663 collaboration. Extrapolations of costs, systematic errors, feasibility, risks and manpower  
664 issues from the *R&D* phase to the final detector are always subject to large uncertainties.  
665 In consequence, many compromises had to be taken with difficult decisions. A strong  
666 impact came from the potentially available infrastructure and manpower of the interested  
667 institutions and the available funds. Finally in 1994 the agreement has been presented in  
668 the ATLAS proposal [36]. The Fig. 19 shows the layout of the ATLAS calorimeter. For  
669 the barrel hadronic calorimeter the TILE calorimeter option has been chosen, mainly for  
670 funding reasons. The electromagnetic calorimeter was chosen to be the accordeon option  
671 for the full coverage in  $\eta$ . The hadronic endcap calorimeter (HEC) with Cu absorber  
672 structure covers the forward region  $1.5 < |\eta| < 3.2$ . Finally the FCal calorimeter with  
673 tube geometry and Cu (electromagnetic) or W (hadronic) absorber structure covers the  
674 very forward region  $\eta > 3.1$ .

675 The calorimeter group of the institute focused finally on the HEC calorimeter. The  
676 construction work was shared with Canadian (TRIUMF/Vancouver) institutions and a  
677 German-Russian cluster. The preference for Cu rather than Fe as abosorber was mainly  
678 driven by rather cheap plate machinig in Canada due to free capacity of the oil drilling  
679 companies at that times on one side, and free workshop infrastructure in the Russian insti-  
680 tutions. The European cluster, managed by the institute, got in addition strong support  
681 in funding by the European Community for the Russian industry (ISTC) or labs (INTAS).  
682 Thus the 16 mm thick Cu plates could be machined with the required precision in planarity  
683 and thickness. Also the concept of 'active pads' has been realized with the electronics in  
684 cold. The production of the electronics, which is after installation no more accessible,  
685 required an incredible carefulness in quality control: each chip (IC) prior to assembly has  
686 been cold tested, as well as the final PC boards and last not least the fully assembled stacks  
687 with the electronics. A large fraction of the modules has been actually tested at CERN in  
688 beams, providing important information for the calibration. The Fig.20 shows one HEC  
689 wheel on the assembly table prior to the vertical rotation. Finally one of the highlights of  
690 the LHC results and the ATLAS LAr calorimeter was the detection of the Higgs Boson H,  
691 and here in particular the decay  $H \rightarrow \gamma\gamma$ . The high precision measurement of the energy  
692 and direction of the  $\gamma$  offers a large discovery potential even in a harsh environment. The  
693 Fig. 21 shows the effective mass  $m_{\gamma\gamma}$  of two  $\gamma$ 's after background subtraction. Shown is  
694 the distribution for the discovery data as well as for the higher luminosity run 2 data.

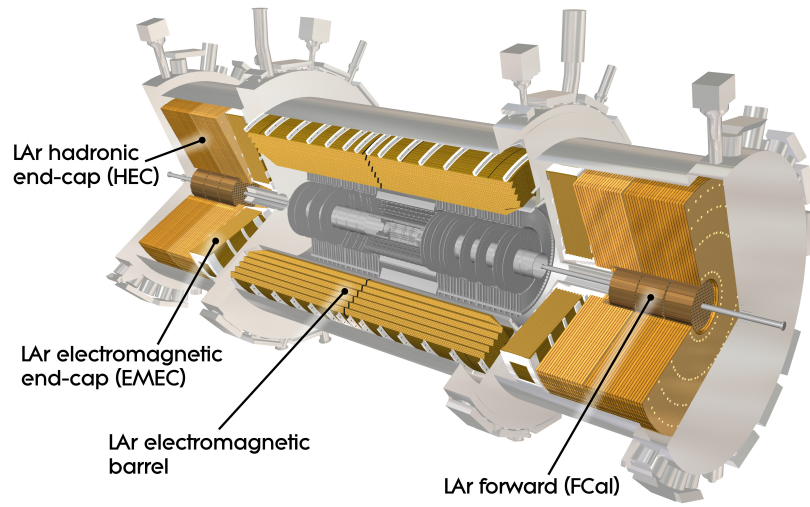


Figure 19: View of the ATLAS calorimeter system. Shown are the electromagnetic and hadronic sections in the barrel as well as in the end-cap.

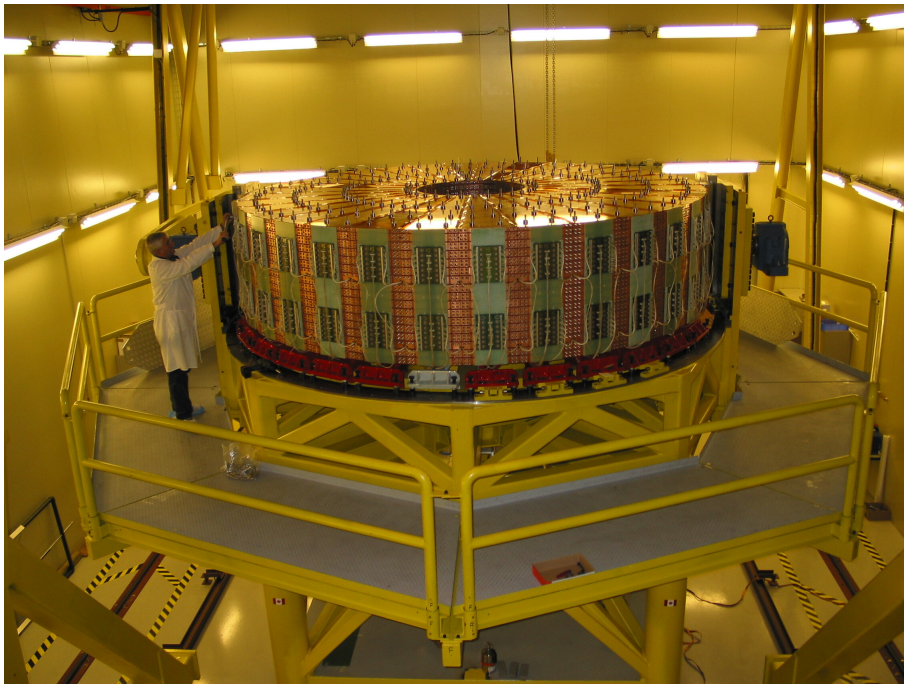


Figure 20: One HEC wheel on the assembly table prior to the vertical rotation and insertion into the end-cap cryostat.

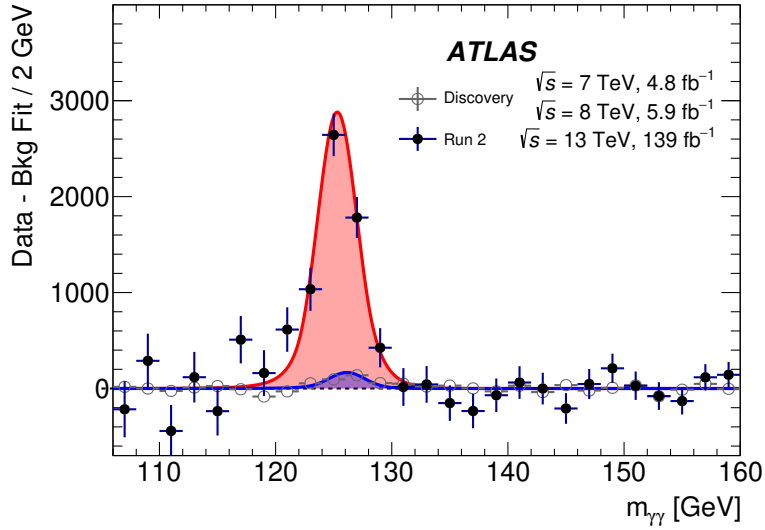


Figure 21: The decay of the Higgs boson  $H \rightarrow \gamma\gamma$ . Shown is the effective mass  $m_{\gamma\gamma}$  of two  $\gamma$ 's after background subtraction for the discovery data set and for the higher luminosity run 2 data.

### 695 4.3 The Future: from ATLAS at LHC/HL-LHC to the Future Circular 696 Collider (FCC)

697 Presently ATLAS is upgrading the detector for higher luminosities expected at HL-LHC.  
698 But already the LHC luminosities triggered many optimization strategies to mitigate the  
699 pile-up in the calorimeter reconstruction of particles and jets. Using the tracking infor-  
700 mation or the timing information from calorimeter signals proved to be very successful.  
701 Thus for jets - after hadronic weighting - an energy resolution has been obtained for the  
702 transverse momentum  $p_{\perp}$  of  $\sigma_{p_{\perp}}/p_{\perp} = 23\% \oplus 2\%$  at 20 GeV or  $\sigma_{p_{\perp}}/p_{\perp} = 6\% \oplus 0.5\%$  at  
703 300 GeV.

704 In a next step jets are being reconstructed using both, the calorimeter as well as the track-  
705 ing information. Thanks to the fine segmentation of the LAr calorimeter this approach  
706 turns out to be very promising. For jets with  $p_{\perp} < 50 \text{ GeV}$  the energy resolution can be  
707 further improved by 10% - 20%.

708 The FCC is the future collider project at CERN, designed for 100 TeV in the hadron  
709 collider version (FCC - hh) or 90 - 400 GeV in the  $e^+e^-$  version (FCC - ee). With the FCC  
710 - hh planned at present the peak luminosity will increase further to  $\mathcal{L} = 3 \times 10^{35} \text{ cm}^{-2} \text{ s}^{-1}$ .  
711 In addition the higher energies yield larger boosts for jets. Physics at the EW scale is  
712 asking for high precision at lower energies in the range up to  $\sim 100 \text{ GeV}$ . On the other  
713 side at the high energy frontier a precision reconstruction of leptons and jets is required  
714 as well. Thus typical calibration signals as obtained from Z decays have to be scaled up  
715 few orders of magnitude. Both, the option to combine the calorimeter measurement with  
716 the tracker information as well as the large range in energy can be matched with the LAr

717 technology: fine segmentation of the calorimeter and the excellent linearity and stability  
718 of the signal.

719 First concepts of a future FCC detector have been studied [37]. Following somewhat the  
720 ATLAS concept, the barrel electromagnetic calorimeter as well as the forward electromag-  
721 netic and hadronic calorimeters are in LAr technology. For the barrel electromagnetic  
722 Pb-calorimeter a non-standard absorber plate orientation with respect to the particle im-  
723 pact angle has been chosen: in  $\phi$  the absorber plates are tilted by  $50^\circ$  with respect to the  
724 particle impact. This is somewhat similar to the TGT approach, but here the 'turbine'  
725 has been realized in  $\phi$  rather than in  $\eta$ . This is reasonable due to the rather limited range  
726 in  $\eta$ . As in the TGT concept, this allows for a very homogeneous response and offers an  
727 optimal segmentation. To stay away from the critical ionization limit the gap width has  
728 been set to  $1.15\text{ mm}$ . In the forward region  $|\eta| > 1.5$  a planar geometry has been chosen.  
729 Here the gap is further reduced, up to  $0.5\text{ mm}$  for the electromagnetic calorimeter in the  
730 region  $|\eta| < 2.5$ . For the very forward calorimeter  $|\eta| < 6.0$  a gap width of  $0.1\text{ mm}$  has  
731 been chosen. Here the required tolerances as well as radiation hardness of all the materials  
732 used, need a dedicated *R&D* study.

733 It is evident that the requirements in FCC on calorimetry are challenging. The LAr  
734 technology has a big potential to fulfil these requirements, eventhough detailed studies are  
735 needed before a final detector can be proposed.

## 736 5 Muon Detection at Colliders

### 737 5.1 The Muon Spectrometer of the ATLAS Experiment at the LHC

738 Muon detection with high efficiency is of special importance for the physics program  
739 at high-energy proton colliders, in an environment with high particle and hadron jet  
740 multiplicities. This is in particular true for the Large Hadron Collider (LHC), the world's  
741 highest energy collider, where the experiments attempt to detect extremely rare processes  
742 in an overwhelming hadronic background. High muon detection efficiency and momentum  
743 resolution was essential for the discovery of the Higgs boson at the LHC, its main goal, in  
744 the decay  $H \rightarrow ZZ^* \rightarrow \mu^+\mu^-\mu^+\mu^-$  into four muons through two  $Z$  bosons decaying in to  
745 oppositely charged muon pairs. High muon momentum resolution up to muon energies of  
746 around 1 TeV is required for searches for new physics processes beyond the Standard model  
747 like decays of a heavy partner  $Z'$  of the  $Z$  boson into muon pairs or of supersymmetric  
748 partners of the Standard Model particles.

749 The design of the ATLAS detector (Figure 22)[39] pays special attention to precise and  
750 stand-alone muon measurement which was particularly emphasized by the MPP group  
751 when the experiment was founded. The muon spectrometer in a superconducting air-core  
752 magnet minimizing scattering material for the muons is a novelty for a collider experiment  
753 and distinguishes the ATLAS detector (Fig. 22) from the other LHC experiments. It allows  
754 for high muon momentum resolution over a wide energy range from 5 GeV to 1 TeV



755 independent of other subdetectors. The name ATLAS, acronym for "A Toroidal LHC  
 756 Apparatus", is derived from this outstanding feature. The MPP group strongly promoted  
 757 such a detector concept, and initiated for this purpose a new detector proposal for the  
 758 LHC in the early 1990s, called ASCOT ("Apparatus with SuperCONducting Toroids";  
 759 see Fig. 17)[30]. MPP under the department director Friedrich Dydak formed a new  
 760 experimental collaboration for participation at the LHC which included most of the high  
 761 energy particle physics groups in Germany which at the time had still been undecided  
 762 which experiment proposal to join.

763 Soon afterwards, the ASCOT concept was merged with another proposal—called EAGLE  
 764 ("Experiment for Accurate Gamma, Lepton and Energy Measurements"), which also em-  
 765 ployed a liquid argon electromagnetic calorimeter and a toroidal magnetic field for the  
 766 muon detector, although normal conducting and with iron core—to become the ATLAS  
 767 experiment. The superconducting air-core toroid solution was retained for the new AT-  
 768 LAS detector. The independent high-precision momentum measurement in the muon  
 769 spectrometer is especially important for ATLAS compared to its competitor at the LHC,  
 770 the CMS ("Compact Muon Solenoid") experiment, as it has a two times weaker solenoidal  
 771 magnetic field in the central tracking detector than CMS, which relies on the muon mo-  
 772 mentum measurement in the central tracker.

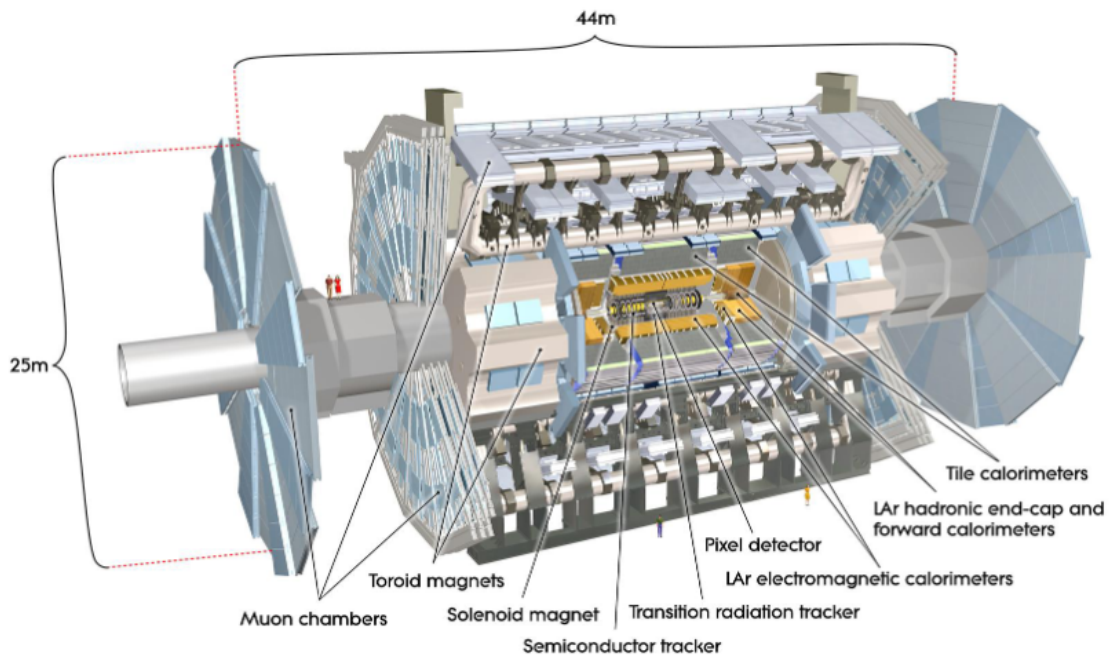


Figure 22: Cut-away view of the ATLAS detector dominated by the muon spectrometer with the barrel and endcap toroid magnets (grey) and the muon detectors (light blue) mounted on them. The muon spectrometer encloses the electromagnetic (orange) and hadronic (grey-green) calorimeters and the central tracking detectors (brown) which together are of the size of the ALEPH detector (chapter 2).

773 There are several unprecedented challenges for the ATLAS muon spectrometer under the  
 774 experimental conditions at the LHC which were considered insurmountable by a large part



775 of the high-energy physics community at the time. In order to achieve the desired 10%  
 776 momentum resolution at the highest energies, the lever arm for measuring the muon track  
 777 curvature in the magnetic field needed to be large, 6 to 10 m, making the superconducting  
 778 magnet coils and the muon detection area huge, about  $5500 \text{ m}^2$ , equivalent to the size of  
 779 a soccer field. Therefore, the muon spectrometer [40] determines the size of the ATLAS  
 780 detector making it the largest collider experiment ever built, with a diameter in the central  
 781 part of 25 m and a length of 40 m between the outer detector layers (Fig. 22).

782 The large detection area had to be instrumented with roughly 1200 muon detectors with  
 783 unprecedentedly high spatial resolution of  $40 \text{ }\mu\text{m}$ , positioned in the vast spectrometer  
 784 volume with similar precision. Additionally, the muon chambers have to cope with un-  
 785 precedentedly high background radiation rates of low-energy neutrons and gamma rays  
 786 which are created in the interactions of high-energy particles from the proton collisions  
 787 in the calorimeters and the shielding material around the beam pipe of the LHC. The  
 788 background radiation dominates the hits in the muon chambers by orders of magnitude.  
 789 It not only deteriorates the muon detection efficiency and spatial resolution but can also  
 790 cause aging of the detectors making them unusable over the foreseen long lifetime of the  
 791 experiment of initially 10 years at the LHC and now in total 25 years, including operation  
 792 at the high-luminosity upgrade HL-LHC starting in 2029. As most of the muon chambers  
 793 can never be replaced and are very difficult to access for repairs, they need to be highly  
 794 reliable.

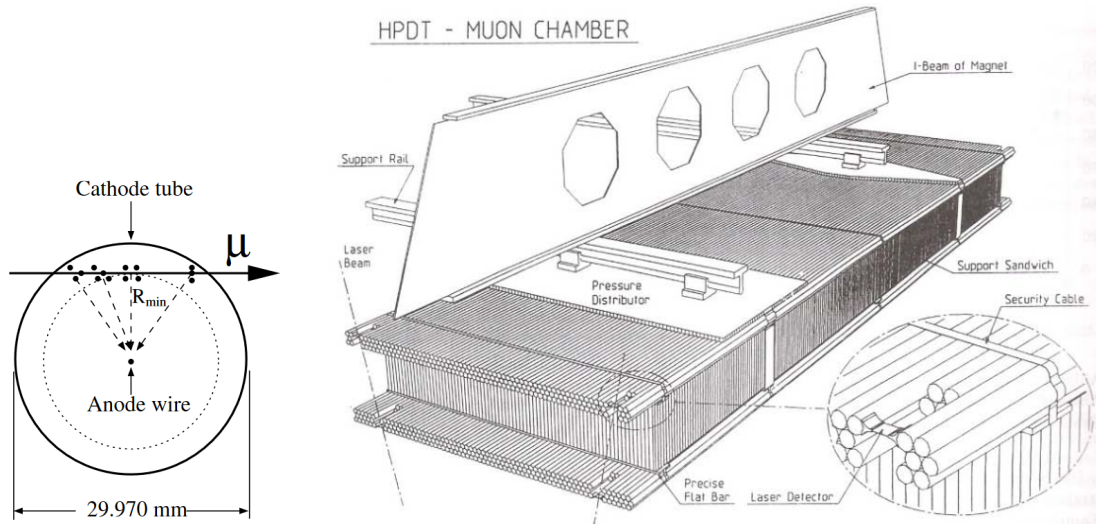


Figure 23: Left: Working principle of a drift tube: The ionization electron clusters created along the muon path in the gas drift in the electric field towards the anode wire. The drift time measured by the readout electronics is a measure of the distance of the muon track from the known wire position. Right: High Pressure Drift Chamber (HPDT) concept of MPP for the ASCOT and ATLAS experimental proposals [39] [?]. Several layers of drift tubes on either side of a support structure combine to measure a muon track segment with 40 spatial resolution if the sense wire position uncertainty can be neglected.

795 **5.2 The Muon Drift Tube Detectors**

796 The MPP group set out early on to design such robust high-precision muon tracking de-  
 797 tectors. To cover the large areas at acceptable cost, gas chambers are the only option. It  
 798 was realized that high mechanical precision and stability of the chambers was required.  
 799 The MPP group, with Walter Blum as prominent representative, developed and strongly  
 800 promoted the High-Pressure Drift Tube (HPDT) concept (Fig. 23) for the ASCOT experi-  
 801 ment proposal [?] which was finally adopted by ATLAS in a fierce competition with several  
 802 other proposals in the form of the Monitored Drift Tube (MDT) chambers, illustrated in  
 803 Fig. 24. This was a great success for the MPP group; the acronym "MDT" was jokingly  
 804 interpreted as "Munich Drift Tubes". In the following, the MDT chambers and the optical  
 805 alignment monitoring system for the ATLAS muon spectrometer were designed at MPP,  
 806 the first prototypes built and the largest detector construction project in the history of  
 807 MPP brought on the way.

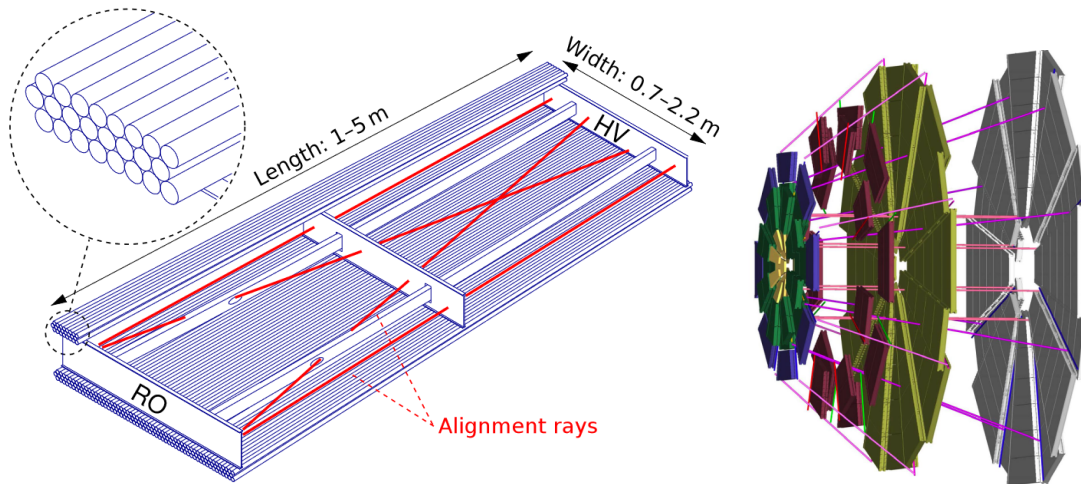


Figure 24: Left: ATLAS MDT chamber concept with light support frame containing the planarity monitoring system using light rays and optical position sensors. Right: Impression of the light ray network connecting the MDT chamber layers of one endcap muon spectrometer.

808 The ATLAS MDT chambers consist of two triple or quadruple layers of 30 mm diameter  
 809 aluminum tubes separated by a light-weight support structure into which an optical pla-  
 810 narity monitoring system is integrated. In total there are almost 140000 drift tubes in the  
 811 ATLAS muon spectrometer. The tubes have only  $400 \mu\text{m}$  thick walls and are filled with  
 812 Argon gas with an admixture of 7%  $\text{CO}_2$  at two bar overpressure. A voltage of 3080 Volt  
 813 is applied between the aluminum tube wall and the  $50 \mu\text{m}$  thin anode wire in the center of  
 814 the tube. These so called drift tubes measure the time it takes for the ionization electrons  
 815 created along the traversing muon tracks to drift to the anode wire in the radial elec-  
 816 tric field (Fig. 23). In the region of high electric field near the wire, secondary ionization  
 817 avalanches multiply the charge by a factor of 20000 which is well detectable by the readout  
 818 electronics connected to the wire. The drift time is a measure of the distance of the muon  
 819 track to the sense wire. The drift detector principle allows for high spatial resolution with  
 820 a minimum number of expensive electronic channels. The gas over-pressure significantly

821 reduces the statistical fluctuations in the arrival time of the ionization electrons.

822 The individual MDT drift tubes achieve a spatial resolution of  $80\ \mu\text{m}$ . Combination of  
823 the measurements in 6 to 8 drift tube layers along the muon track leads to the required  
824 spatial resolution of  $40\ \mu\text{m}$ . This requires that the several hundred sense wires in a chamber  
825 are positioned with an accuracy of  $20\ \mu\text{m}$ , a mechanical precision which had never been  
826 achieved before on such a large scale. Initially, there was a wide-spread believe in the High  
827 Energy physics community that this would never be feasible.

828 Muon tracks are measured in the toroidal magnetic field in three layers of MDT chambers,  
829 the minimum for determining the muon momentum from the track curvature. For muons  
830 with 1 TeV energy the deviation of the tracks from a straight line over the distances of 6  
831 to 10 m inside the muon spectrometer is only  $100\ \mu\text{m}$ . In addition to the high mechanical  
832 precision of the individual MDT chambers, their relative positions in the three layers  
833 of muon chambers, therefore, have to be known with similar precision of  $30\ \mu\text{m}$  at all  
834 times. This could only be achieved by continuously monitoring the relative MDT chamber  
835 positions at this level of precision using optical position sensors mounted on the chambers  
836 which are connected by a network of hundreds of light rays (Fig. 24). The optical alignment  
837 system was proposed and to a large extent developed by the MPP group under Hubert  
838 Kroha, then still a postdoc at MPP with limited contract. The development was funded  
839 by an INTAS program of the European Union. The design fulfilled the high expectations  
840 which originally appeared almost impossible to achieve for such a large detector system.

841 A whole sector of the muon spectrometer with MDT chambers and alignment monitoring  
842 system was tested in real size with muons from cosmic rays and from a high-energy beam  
843 of the Super Proton Synchrotron (SPS) at CERN under MPP coordination (see Fig. 26).  
844 This system test was essential for the successful installation and operation of the ATLAS  
845 muon spectrometer.

### 846 **5.3 MDT Chamber Construction**

847 The about 1200 MDT chambers for ATLAS with almost 140000 drift tubes were produced  
848 in a world-wide collaboration of 11 particle physics institutes over a period of 5 years  
849 between 2001 and 2006. The MDT chambers turned out to be reliable beyond expectations  
850 with only a handful of wires broken so far and no signs of aging effects. This was achieved  
851 by enforcing common strict quality criteria at all construction sites under the coordination  
852 of the MPP group. The drift tubes and chambers had to be assembled in clean rooms. The  
853 drift tube materials had to be carefully selected, and strict cleanliness had to be ensured  
854 at all times in order to avoid contamination of the drift gas which could lead to deposits on  
855 the sense wires, so called wire aging, under the unprecedentedly high background radiation  
856 doses at the LHC.

857 MPP accepted the responsibility for the construction of the 88 MDT chambers in the  
858 outermost layer of the central cylindrical (so called barrel) part of the muon spectrometer,  
859 comprising 37000 drift tubes altogether and covering an area of  $700\ \text{m}^2$ . The chambers  
860 consist of two triple layers of drift tubes of four meter length and are more than two meters

861 wide (see Figure 6). They each contain about 430 drift tubes. MPP also supported the  
862 MDT chamber construction at the Joint Institute for Nuclear Research (JINR) in Dubna,  
863 north of Moscow, in the framework of a program of the European Union to support  
864 russian research institutes (INTAS) which allowed JINR to make its contribution to the  
865 construction of the ATLAS muon spectrometer. The MPP installed a clean room with  
866 an automated drift tube assembly station to produce the drift tubes both for the MDT  
867 chambers from JINR and from MPP (Fig. 26).

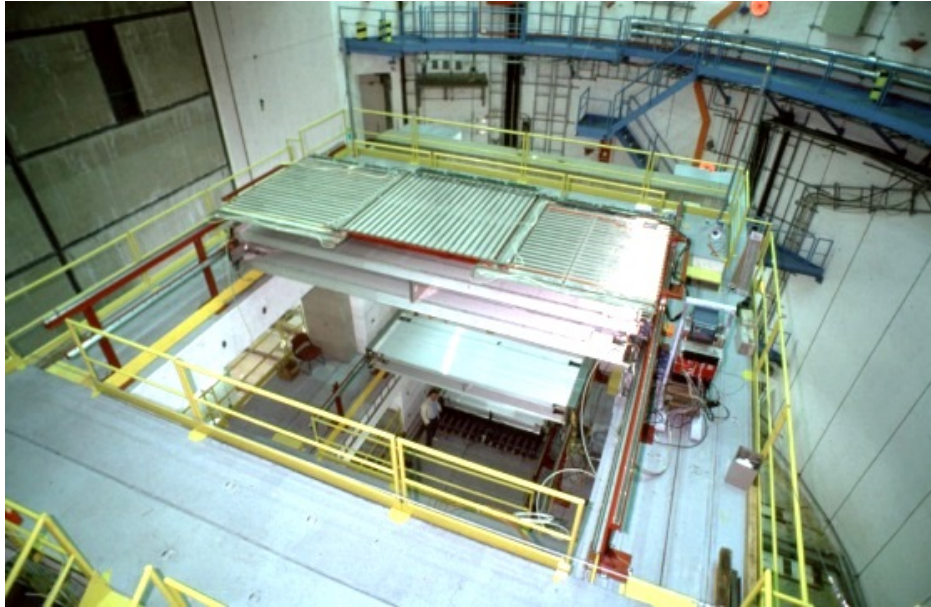


Figure 25: ATLAS muon system teststand at CERN in the former experimental hall of the UA1 experiment, installed and operated by Hans Dietl from MPP (on the floor at the bottom) from 1996 until 2000. The teststand consisted of a real-size sector of the ATLAS barrel muon spectrometer with three layers of prototype MDT chambers in operation.



Figure 26: Left: Visit of a CERN delegation consisting of the director of research Roger Cashmore and the leader of the theory department John Ellis in the clean room installed by MPP at JINR Dubna in 1999. Right: The clean room with automated drift tube assembly station installed by MPP at JINR Dubna in February 2000.





Figure 27: Left: The first MDT prototype chamber constructed at MPP in the new clean room in February 1998. The chamber dimensions are of the same size as for the series production. Right: Assembly of the first MDT chamber of the series production at MPP with the first prototype chamber in August 2000. The drift tubes of each layer are positioned in precise combs on the granite table. In the picture, the first tube layer has been glued to the support frame which has been lifted from the table. The support frame with glued tube layers can be rotated on the crane in order to successively glue the next tube layers to the top and bottom of the frame. The construction of the 88 chambers required for the outermost barrel layer of the ATLAS muon spectrometer was completed in December 2005.



Figure 28: MDT chamber storage and test with cosmic ray muons during the series production in a large hall rented in the north of Munich while storage space for the chambers was not yet available at CERN.



Figure 29: The team of physicists, engineers and technicians working on the MDT chamber construction and test in July 2001 after completion of 10% of the chambers.

868 The MPP group, under the leadership of Hubert Kroha, lead the design of the MDT  
869 chambers, of the precision construction methods and of the integration in the air-core  
870 toroid magnet from the beginning. The chamber construction method was strongly cou-  
871 pled to the design of the drift tubes themselves. The sense wires are positioned in the  
872 center of externally accessible aluminum rings surrounding the drift tube endplugs with  
873 an accuracy of  $5\ \mu\text{m}$ . This was verified for each tube end with an X-ray method. The  
874 tube endplugs were then placed layer by layer in combs also mounted with  $5\ \mu\text{m}$  precision  
875 on a polished granite table in a temperature controlled clean room (see Fig. 27). The  
876 fabrication of highly precise mechanical tools for the assembly of such large objects was  
877 new territory at the time. The development consequently took 5 years. The tube layers  
878 were alternately glued to the top and the bottom side of the support frame which was  
879 lowered to the combs for glueing and then lifted and turned around on a crane. During  
880 glueing together two adjacent tube layers, the gravitational deformations of the support  
881 frame on the crane had to be compensated with hydraulic pistons.

882 The sense wire positions are fixed relative to each other at the drift tube ends by the  
883 chamber assembly combs. Along the whole length of the tubes, the wire positions can  
884 then be predicted by precisely adjusting the wire tension during the drift tube assembly  
885 which determines the gravitational sag of the wire. The sag of the drift tube layers of each  
886 chamber under their own weight, monitored by the optical planarity measurement system  
887 (Fig. 24), was adjusted to the smaller wire sag using a mechanical strain mechanism in  
888 the support frame.

889 The MPP group designed and constructed the first MDT prototype chamber in 1998  
890 (Fig. 27) [41], shortly after completion of the Technical Design Report for the Muon  
891 Spectrometer in September 1997, which was the result of a development period of five  
892 years. By scanning this prototype chamber with X-rays at CERN, it was demonstrated  
893 for the first time [41] that the required mechanical precision in the sense wire positioning  
894 of better than  $20\ \mu\text{m}$  could be achieved, allowing for the start of the MDT chamber series  
895 construction. Spot checks with the X-ray scanner of chambers from all construction sites  
896 confirmed the precision over the whole production period.

897 A completely new infrastructure with large temperature controlled clean room, large highly  
898 precise granite tables (Fig. 27) and and a large coordinate measuring machine for the  
899 verification of the mechanical precision had to be installed for the construction of such  
900 large and mechanically precise detectors. This was possible because of the strong support  
901 of the project by the managing director of the institute at the time, Volker Sö rgel. A large  
902 storage hall outside Munich had to be rented for the chambers during the series production  
903 (Fig. ??) because storage space for the chambers was not yet available at CERN. The  
904 functionality of the chambers over the long storage time was tested and analysed by many  
905 master and graduate students enthusiastic for the ATLAS project.

906 Several university grade mechanical engineers were hired for this project, a novelty for the  
907 institute's design office at the time, but indispensable for the complex engineering tasks in  
908 a complex environment like the ATLAS detector performed in international project teams.  
909 One of them, Klaus Fritsch, became project engineer of the ATLAS muon spectrometer  
910 project. Unfortunately he left the institute for another job just before the start of the  
911 MDT chamber series construction. The specially complex chambers with cutouts in the  
912 rectangular shape for letting cables passing through were then designed by a physicist,  
913 project leader Hubert Kroha himself.

914 The construction of the 88 MDT chambers of 2 m x 4 m size at MPP took five years  
915 from January 2001 to December 2005. This was the by far largest detector construction  
916 project in the history of MPP. During peak time, more than 15 technicians worked on the  
917 project. The team of technicians (Fig. 29) was coordinated by Alexander Wimmer who  
918 later became the head of the mechanical workshop. The competence of the institute's  
919 engineers and workshops was essential for the success of the MDT project and of the  
920 ATLAS detector construction as a whole. It was a challenge to maintain or even increase  
921 the level of competence for future projects.

922 In parallel to the chamber construction, the MPP group operated chambers in the system  
923 test stands with high-energy muon beams and in the Gamma Irradiation Facility at CERN.  
924 In the latter, the performance of complete MDT chambers under the irradiation conditions  
925 expected during the operation of the ATLAS detector at the LHC was evaluated. The  
926 studies showed the capability of the chambers to cope with the high background counting  
927 rates at the maximum LHC beam collision intensity, but also the limitations of the 30 mm  
928 diameter drift tubes in the case of an upgrade of the LHC to considerably higher proton  
929 collision rates.

930 The MDT chambers were integrated at CERN with dedicated gas detectors with high





Figure 30: Integration of the MPP MDT chambers with RPC trigger chambers and commissioning in a dedicated hall at CERN before installation in the ATLAS detector. Top left: MDT chamber storage at CERN. Top right: RPC chambers prepared for the integration with the MDT chambers in support frames designed and constructed at MPP. The distance between MDT and RPC chambers in the package had to be adjusted with millimeter precision under the same inclination angle as in the muon spectrometer to make the installation in the small available space possible. The rotation stand used for this purpose is visible at the top left in the picture at the bottom. The row of completed combined detectors can be seen in the foreground.



Figure 31: Top Left: Installation of an MDT chamber on the outside of a barrel toroid magnet cryostat at the top of the ATLAS detector. The chambers had to be lowered to the ATLAS cavern, inserted on rails mounted on the toroid coils and positioned with millimeter precision. Top right: Installation team of the MPP MDT chambers in the "feet" region of the barrel muon spectrometer on the floor of the ATLAS experimental cavern. Bottom: Fine adjustment of an MDT chamber in the ATLAS muon spectrometer by a young female technician from MPP working in climbing harness at large height and in very cramped space.



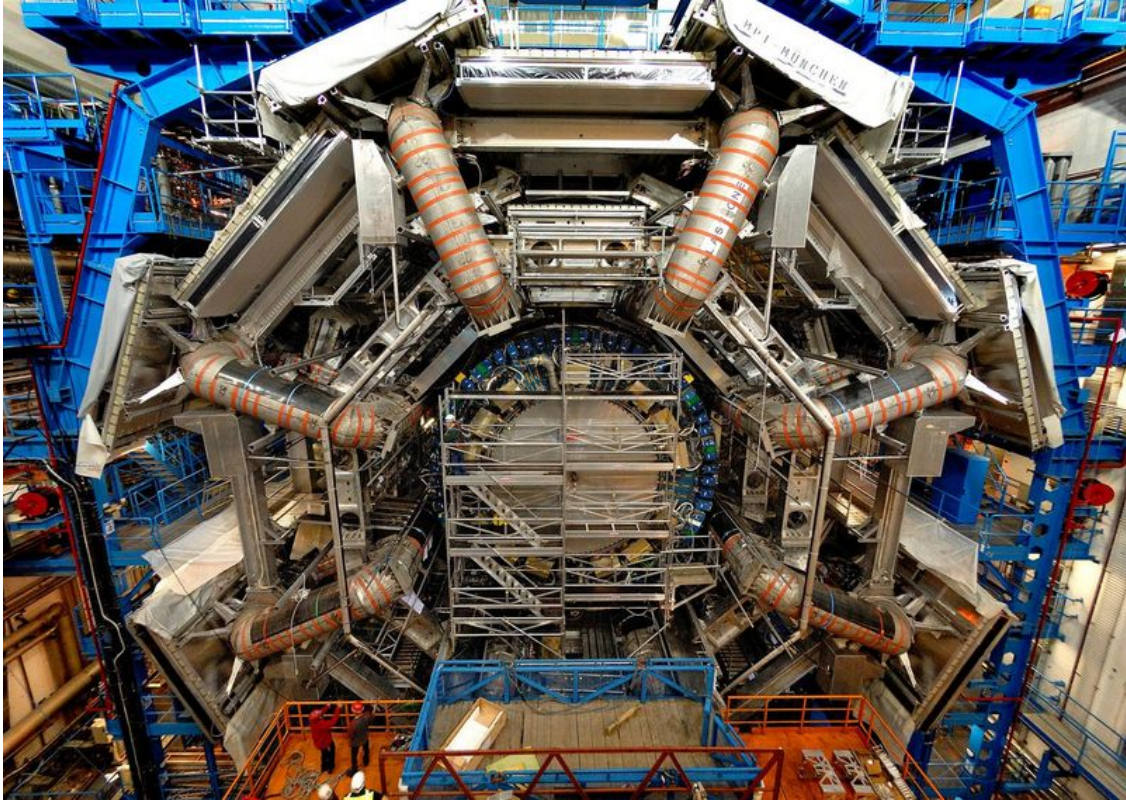


Figure 32: Completion of the barrel MDT chamber installation in June 2006. The MPP chambers are located in the outermost layer protected by covers. The enormous size of the ATLAS detector with a diameter of 25 m is apparent. The MPP PhD students, enthusiastic to help commission the chambers in the ATLAS cavern, expressed the pride in their work by installing a sign "MPI München" on a chamber well visible at the top right of the ATLAS detector in a height of 25 m.

931 time resolution (Resistive Plate Chambers, RPC), which deliver fast muon trigger signals  
932 for the readout of the MDT chambers, during one year between July 2005 and May  
933 2006 (Fig. 30). The installation and commissioning of the MPP chambers in the ATLAS  
934 muon spectrometer took place from February to June 2006 (Fig. 32). The chambers had  
935 to be lowered individually through the access shaft to the ATLAS cavern 100 meters  
936 underground where they were shifted onto rails mounted on the toroid magnet cryostats  
937 and brought into their nominal positions with millimeter accuracy. The MPP installation  
938 crew consisting of physicists, engineers and technicians gathering at the ATLAS cavern  
939 floor is shown in Fig. 31.

#### 940 5.4 Muon Drift Tube Chambers for the Highest Counting Rates

941 Already before the start of the ATLAS MDT chamber construction, considerations of a  
942 possible increase of the maximum proton collision intensity (luminosity) of the LHC by  
943 up to an order of magnitude got on the way. The upgraded version of the LHC was

944 originally called Super-LHC (S-LHC), and later approved as High-Luminosity LHC (HL-  
945 LHC) in 2016 to start operation in 2029 after several steps of improvements. Based on  
946 the measurements of MDT chambers in a muon beam under high background irradiation  
947 at the Gamma Irradiation Facility at CERN performed by the MPP group from 2003  
948 on, it became clear that the MDT chambers in the inner endcap layers and parts of the  
949 inner barrel layer would not be able to cope with the background counting rates increasing  
950 proportionally to the proton collision rate and consequently needed replacement.

951 At the same time, muon trigger chambers were needed also in the inner muon spectrom-  
952 eter layer to reinforce the muon trigger efficiency. The readout electronics of the MDT  
953 chambers had to be upgraded to cope with the higher trigger and data rates at HL-LHC.  
954 This would allow for a new continuous readout and MDT based trigger scheme, which was  
955 proposed by MPP [42] in order to improve the momentum resolution of the muon trigger  
956 in order to control the trigger rate of low momentum muons. The dedicated ATLAS muon  
957 trigger chambers, Resistive Plate Chambers (RPC) in the barrel and Thin Gap Chambers  
958 (TGC) in the endcap regions [39], provide much lower spatial and momentum resolution  
959 than the MDT chambers.

960 From 2008 on, the development of a new generation of precision muon tracking detec-  
961 tors with higher rate capability, sufficient for HL-LHC and potential future colliders, was  
962 advanced at MPP under the leadership of Hubert Kroha. This development led a few  
963 years later to another large-scale construction project for the upgrade of the ATLAS de-  
964 tector at HL-LHC. It turned out that the counting rate capability of the drift tubes can  
965 be improved by an order of magnitude [43], sufficient for operation at HL-LHC and fu-  
966 ture highest-energy proton colliders conceivable in this century, by reducing the drift tube  
967 diameter by a factor of two while maintaining the MDT operating parameters like gas  
968 composition, pressure and amplification, and by improving the signal processing of the  
969 readout electronics to avoid degradation or loss of the muon signals due to preceding  
970 background signals.

971 In the course of these developments, the custom design of integrated circuits in modern  
972 chip technologies was established at MPP. With this competence, the MPP ATLAS group  
973 successfully developed the new readout chips for the ATLAS MDT chambers for the HL-  
974 LHC upgrade well before the official start of the ATLAS upgrade project [?]. The MDT  
975 readout chips are now being further developed for higher counting rates at future colliders  
976 and in modern chip technologies (Fig. 33).

977 The new drift tube chambers, known as small-diameter Muon Drift Tube (sMDT) cham-  
978 bers [43], have become a world-wide trade mark of MPP. They are one of the rare cases  
979 where the complete detector system, including dedicated readout electronics, has been  
980 designed by one and the same institute. With their high reliability and robustness as well  
981 as high background counting rate capability (far beyond HL-LHC requirements), they  
982 constitute ideal, cost effective muon precision tracking detectors for experiments at future  
983 high-energy proton colliders even beyond the HL-LHC.

984 With improved drift tube design for the smaller diameter, drift tube production became  
985 considerably cheaper and chamber assembly faster and more precise. A record sense wire

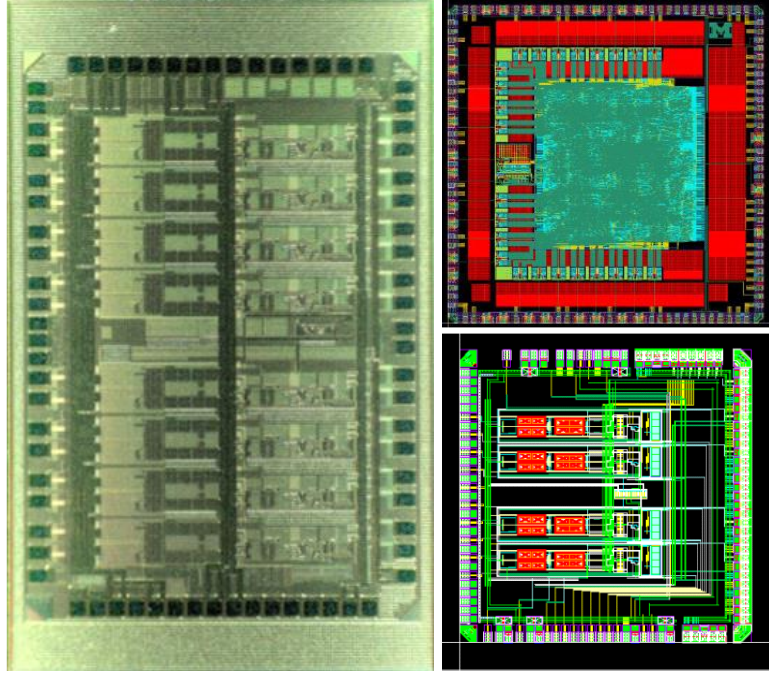


Figure 33: Examples of integrated circuit chips developed at MPP. Left: X-ray picture of the new readout chip for the MDT chambers at HL-LHC with eight channels in 130 nm CMOS technology. Top right: Time-to-digital converter chip for digitization of MDT drift time measurements at HL-LHC in 130 nm CMOS technology. Bottom right: Schematic layout of a new faster sMDT readout chip for high counting rates beyond HL-LHC at future colliders with four channels in 65 nm CMOS technology.

986 positioning accuracy of  $5\ \mu\text{m}$  was achieved in the sMDT chamber productions for ATLAS  
 987 described below [43]. In the new sMDT drift tube design, all sense wire positions can be  
 988 measured mechanically on the outside of the tubes at the endplugs using an automated  
 989 coordinate measuring machine. This also allows for measuring potential mechanical tor-  
 990 sion of the chambers around the tube direction to verify the predictions from the optical  
 991 planarity monitoring system (Fig. 24).

## 992 5.5 Upgrades of the ATLAS Muon Spectrometer

993 The sMDT chambers immediately proved to be very versatile for complementing the AT-  
 994 LAS muon spectrometer in regions which could not be covered with detectors before. In  
 995 total 22 sMDT chambers of different sizes and shapes were designed and constructed at  
 996 MPP (Fig. 35) and installed for operation in ATLAS in 2013, 2016 and 2020 (Fig. 38) [43],  
 997 before the upcoming upgrade for HL-LHC. A new semi-automated sMDT drift tube as-  
 998 sembly facility was established for this purpose at MPP (Fig. 34). The sMDT chamber  
 999 construction for the ATLAS upgrades already required only one third of the person power  
 1000 needed for the MDT chamber production. The sMDT team of physicists and technicians  
 1001 in summer 2022 is shown in Fig. ???. The aim for the future is to completely automatize  
 1002 the drift tube and chamber assembly procedures. To make this development possible,





Figure 34: Clean room at MPP for the semi-automated assembly of the drift tubes of the sMDT chambers. The wires are fed through the tubes using air flow to avoid any manual contact and are tensioned with high reproducibility to guarantee equal gravitational sag of the wires in all tubes within 4%.

1003 new high-level mechanical and electronics engineering capacity had to be acquired for the  
1004 institute. Having achieved this is a milestone in the development of the Technical Depart-  
1005 ment of MPP and will be instrumental for further leadership in detector development and  
1006 construction for future international collider experiments.

1007 The upgrade of the ATLAS detector for HL-LHC initially focussed mostly on the replace-  
1008 ment of the silicon tracking system. The MPP group was the first one to point out early  
1009 on the necessity of also an upgrade of the muon spectrometer which considerably improved  
1010 the muon tracking and trigger efficiency under the expected 10 times higher background  
1011 rates and extended the coverage of the solid angle around the proton-proton collision re-  
1012 gion in detector center [40]. The MPP upgrade proposal first resulted in the replacement  
1013 of the two 20 m diameter wheels of the inner detector layers in the endcap regions of the  
1014 muon spectrometer, completed in 2022.

1015 The main muon detector upgrade for HL-LHC, which was approved by the ATLAS col-  
1016 laboration in 2017, comprises a complete replacement of the innermost layer of MDT  
1017 chambers in the barrel region by sMDT chambers integrated with a new generation of  
1018 RPC trigger chambers and the use of the MDT and sMDT chambers in the muon trigger  
1019 system. The latter serves to improve the muon momentum resolution for the trigger deci-  
1020 sion by an order of magnitude compared to using the RPC chambers alone. It requires the  
1021 replacement of the MDT chamber readout electronics and, thus, the design of new readout  
1022 chips which has been carried out at MPP [45]. MPP also developed the new MDT muon  
1023 trigger processors which for the first time perform muon track reconstruction in real time



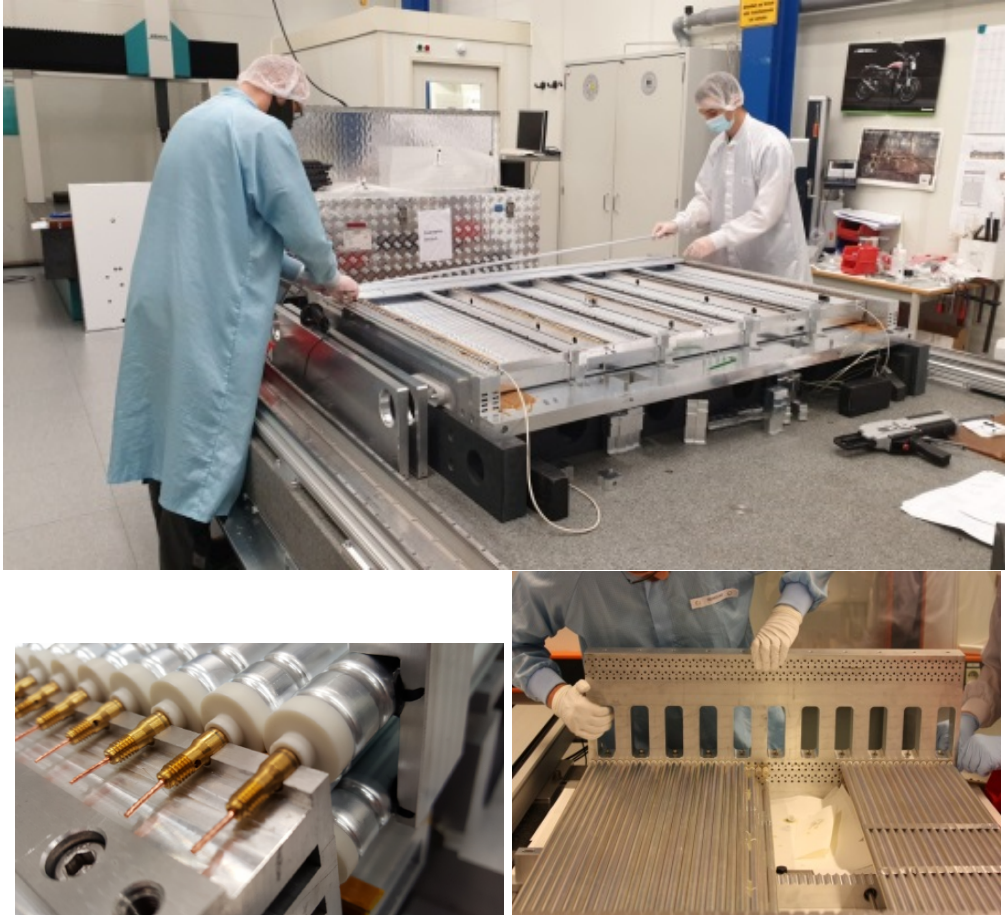


Figure 35: sMDT chamber assembly at MPP. The drift tubes are stacked layer-by-layer on top of each other by inserting the endplugs in precisely machined jigs (bottom) considerably speeding up the assembly procedure and increasing the wire positioning accuracy. The sMDT chamber assembly can be performed by technicians without special training and lends itself for automatization in the future.

1024 within less than a microsecond [46].

1025 For the muon spectrometer upgrade for HL-LHC, Hubert Kroha and the MPP group  
 1026 formed a collaboration of institutes experienced in muon detector construction for the  
 1027 original ATLAS muon detector. The group at the University of Michigan in the United  
 1028 States constructed half of the 96 sMDT chambers needed for the replacement of the  
 1029 MDT chambers in the inner barrel. These chambers were designed and their construction  
 1030 coordinated by MPP. The chamber production at MPP started in January 2021 and  
 1031 was completed in December 2022 as the first ATLAS upgrade project for HL-LHC. The  
 1032 University of Michigan followed 7 months later. The chambers are now all at CERN  
 1033 (Fig. 39), waiting for the installation of the new readout electronics boards designed by  
 1034 MPP and in production, and for the integration with the new RPC chambers. German  
 1035 university intitutes in Munich (LMU), Würzburg and Mainz committed themselves to  
 1036 financing and testing of the sMDT readout electronics boards.



Figure 36: sMDT chambers in various stages of completion in the construction hall in the old MPP building in Munich. After the assembly out of the drift tubes, the gas connections to each individual drift tubes are installed. More than 5000 rubber sealing rings each chamber have to fullfill very high gas tightness standards. By design this worked almost every time in the first attempt. Afterwards, the readout electronics boards and Faraday cages protecting them are installed. The teststand for the final certification test with cosmic ray muons in visible in the background of the pictures.



Figure 37: The team of physicists and technicians working on the sMDT chamber construction and test in March 2023 after completion of the sMDT chamber construction for ATLAS at HL-LHC at MPP.



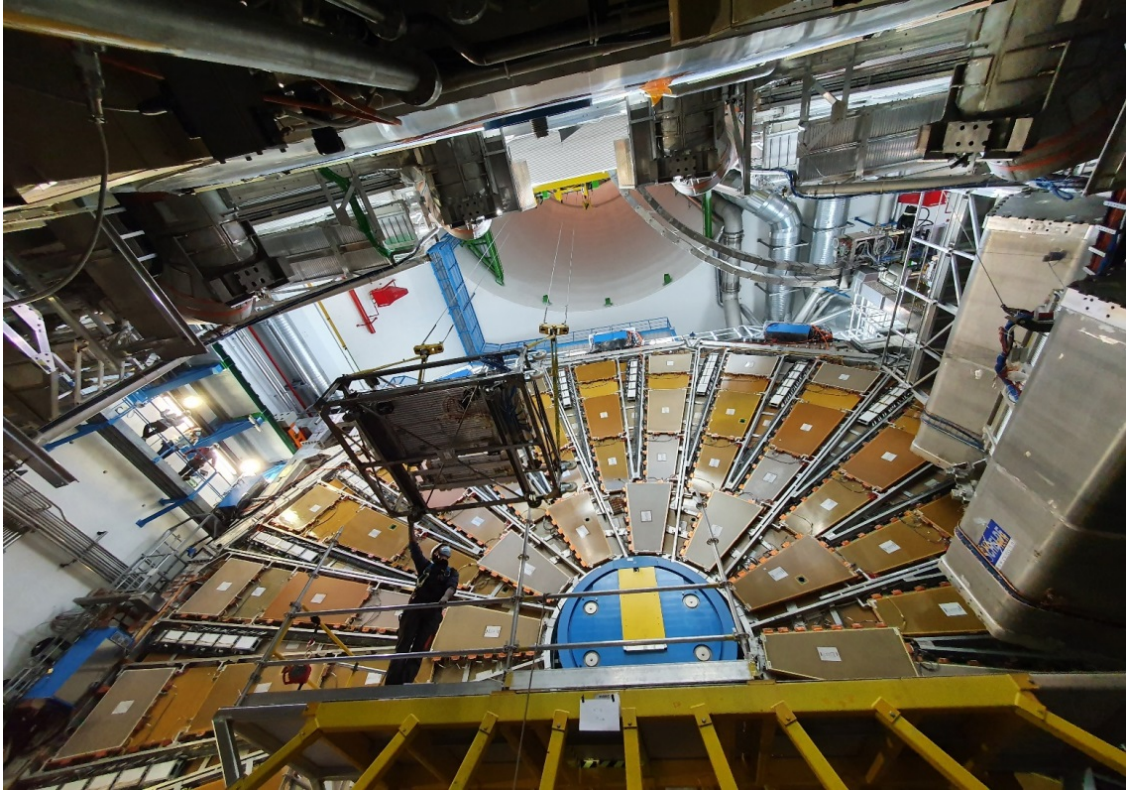


Figure 38: Installation of 8 sMDT chambers in the barrel inner layer of the ATLAS muon spectrometer in the fall of 2020 during a long shutdown of the LHC. The chambers are lowered one by one to the ATLAS cavern 100 m underground, in between the barrel spectrometer and the big wheel of the middle endcap muon chamber layer, which has been retracted for the chamber installation together with the endcap toroid magnet cryostat. The latter is visible on the right edge of the picture taken from the ATLAS cavern floor. The MPP group was one of the few actors at CERN during this critical period.

1037 The Institute for High Energy Physics (IHEP) in Protvino, south of Moscow, played an  
1038 instrumental role for the sMDT chamber construction in providing experienced technicians  
1039 for the drift tube production and testing at MPP from 2017 until February 2021 when  
1040 the collaboration abruptly came to an end. IHEP Protvino also delivered the mechanical  
1041 parts for the sMDT chambers according to the MPP design from a large part of the russian  
1042 funding contribution to the the ATLAS upgrade. The deliveries were completed in April  
1043 2021, in the last possible moment before the borders were closed for trucks from Russia.

1044 MPP also took over the responsibility for the design and production of a quarter of the  
1045 about 1000 new RPC detectors required for the ATLAS muon spectrometer upgrade for  
1046 HL-LHC. Without the engineering contributions of MPP to the RPC project, the upgrade  
1047 of the ATLAS muon spectrometer for HL-LHC could not have been realised. The MPP  
1048 group embarked in the development of new construction methods for the new generation  
1049 of RPC detectors, suitable for reproducible large-scale industrial production. Triplets of  
1050 the new RPC detectors for ATLAS will also be assembled at MPP in mechanical support  
1051 frames designed by MPP. By means of those, the RPC triplets will be combined with the



Figure 39: sMDT chambers built at MPP for the upgrade of the ATLAS muon spectrometer for HL-LHC in the assembly hall at CERN where they are waiting for the delivery and installation of the new readout electronics and for the combination with the new RPC detectors, the construction of which is to start at MPP in 2024.

1052 sMDT chambers before installation in the ATLAS experiment. The design of the RPC  
1053 support frames was challenging because they have to provide enough stiffness to hold the  
1054 stacks of RPC detectors together withing very little space of only 5 cm height in the inner  
1055 barrel layer of the muon spectrometer.

1056 The RPC construction technology has been successfully transferred to two german com-  
1057 panies where the construction for ATLAS will start end of 2024. Together with the new  
1058 RPC construction facility at MPP (Fig. 42), this will be a great asset for the High En-  
1059 ergy Physics community at large to support future large-scale RPC detector construction  
1060 projects. RPC chambers have applications in a wide range of particle physics experiments  
1061 as large-area tracking detectors with high time resolution and moderate cost, from cosmic  
1062 ray detector arrays to collider experiments.

1063 Triplets of the new RPC detectors for ATLAS will also be assembled at MPP in mechanical  
1064 support frames designed by MPP with which they will be combined with the sMDT  
1065 chambers before installation in the ATLAS experiment.

## 1066 5.6 Highlights of Physics with the ATLAS Muon Spectrometer

1067 In parallel with the detector construction and installation, the MPP group prepared for  
1068 the time of the first proton collisions at the LHC and the start of data taking with the  
1069 ATLAS experiment, in order to be at the forefront of the data analysis and potential  
1070 discoveries at the highest center-of-mass energies achieved to date. The first important

1071 step was understanding the operation of the complex detector system and the correct  
1072 interpretation of the data. Years were spent with studies and gradual improvement of the  
1073 simulation of proton-proton interactions in the new uncharted energy regime and of the  
1074 details of the detector response. One of the so called Tier 2 computing centers, used for  
1075 processing and analysis of the ATLAS data, was installed at the computing center of the  
1076 Max Planck Society in Garching and operated by MPP.

1077 The MPP group made decisive developments for the in-situ calibration of the space-to-  
1078 drift time relationship of the MDT chambers in ATLAS and of the muon momentum  
1079 measurement in the muon spectrometer using  $Z \rightarrow \mu^+ \mu^-$  decays as standard candle,  
1080 which are copiously produced at the LHC. For the continuous calibration of the 140000  
1081 MDT drift tubes, a dedicated computing cluster was established at the computing center  
1082 of the Max Planck Society in Garching together with the Tier 2 center.

1083 The high momentum resolution of the ATLAS muon spectrometer is instrumental for  
1084 the efficient detection of the Higgs boson in its decay into four muons. The "golden"  
1085 decay channel  $H \rightarrow ZZ^* \rightarrow \ell^+ \ell^- \ell^+ \ell^-$  into two oppositely charged electron-positron and  
1086 muon-antimuon pairs ( $\ell^+ \ell^-$ ) originating from the decays of two intermediate Z bosons was  
1087 decisive for the discovery of the Higgs boson in July 2012 (Figs. 40 and 41), together with  
1088 the decay into two energetic photons  $H \rightarrow \gamma\gamma$  (see Fig. 21) [48][49]. The discovery took  
1089 place shortly after the start of data taking in 2010, still at proton collision energies of 7  
1090 and 8 TeV which is only half of the design value. The Higgs boson search with the ATLAS  
1091 experiment leading to the discovery was coordinated by Sandra Kortner from the MPP  
1092 group, a former master and graduate student of Hubert Kroha in the ATLAS project now  
1093 leading an independent research group on ATLAS data analysis.

1094 The Higgs boson discovery was confirmed after the increase of the collision energy to  
1095 13 TeV, close to the design value of 14 TeV (Fig. 40) [50]. The high muon momentum  
1096 resolution and precise calibration of the muon spectrometer allowed for the most precise  
1097 measurement of the mass of the Higgs boson in the decay channels into four electrons and  
1098 muons. Together with the precise measurement of the mass of the top quark, the heaviest  
1099 known particle interacting strongest with the Higgs boson, for which the MPP group also  
1100 has been instrumental in the ATLAS experiment, the measurement of the exact mass  
1101 of the Higgs boson is decisive for the range of validity of the Standard Model at energies  
1102 above the LHC.

1103 The MPP group successfully aspired to play an instrumental role in the discovery of the  
1104 Higgs boson, the at the time last undiscovered particle predicted by the Standard Model  
1105 and the main physics target of the experiments at the LHC. In particular, the study of the  
1106 Higgs boson decay into four muons with the aim of identifying possible deviations from  
1107 the Standard Model predictions is a domain of MPP. MPP also plays an important role in  
1108 the precise measurement of the mass of the top quark, the heaviest known particle, with  
1109 which the Higgs boson interacts most strongly.

1110 The new energy regime accessible at the LHC also opened up the opportunity to find other  
1111 new particles predicted by theories extending the Standard Model in order to explain some  
1112 of the many open questions. Extensions with so called Supersymmetry, relating matter

1113 constituent particles to the particles carrying the forces between them, are most promising.  
 1114 Supersymmetry predicts a partner particle for each Standard Model particle. It can explain  
 1115 the small mass of the Higgs boson compared to the expectations from the Standard Model  
 1116 and provides candidates for the particles of Dark Matter in the universe. The search for  
 1117 supersymmetric partner particles decaying into multiple muons was pioneered by MPP.

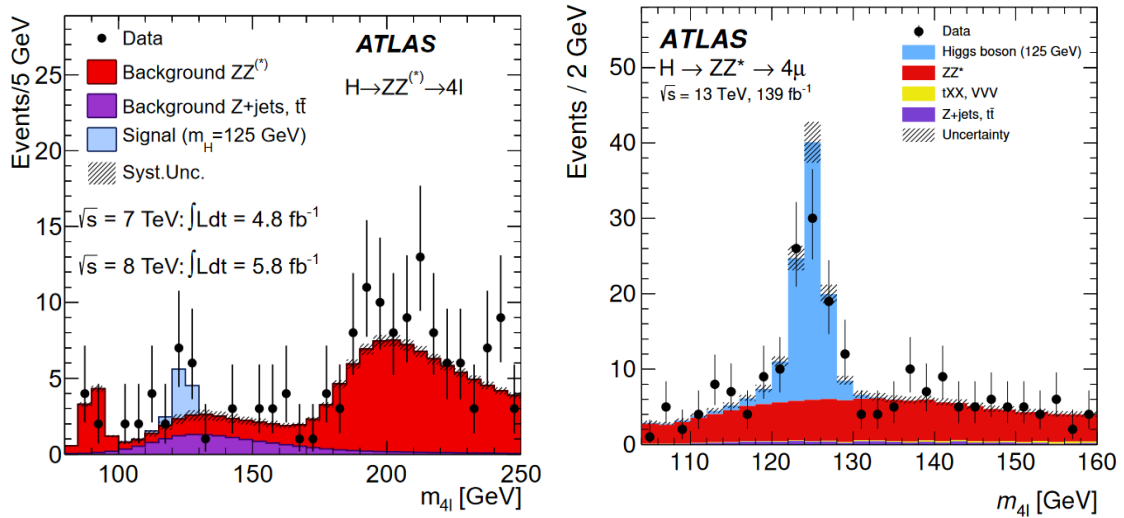


Figure 40: Left: Mass spectrum of four-lepton events contributing to the discovery of the Higgs boson in July 2012 at proton-proton collision energies of 7 and 8 TeV. The excess of events above the expected backgrounds at a mass value of 125 GeV/c<sup>2</sup> indicates the Higgs boson resonance, underlayed by the expectation (light blue) from the Standard Model of Particle Physics [48]. Right: Mass spectrum of four-muon events with 10 times more data from the LHC run at 13 TeV collision energy in the years 2016 to 2018 [50]. The Standard Model expectation for a Higgs boson mass of 125 GeV/c<sup>2</sup> is overlaid in light blue.

1118 The rare decay of the Higgs boson into one oppositely charged muon pair, which requires  
 1119 especially high muon momentum resolution at high energies, is now at the verge of obser-  
 1120 vation at the LHC. The increase of the proton collision rate at HL-LHC by a factor of 5 will  
 1121 allow for the detection of rare Higgs boson decays as well as of possible small deviations  
 1122 of the Higgs boson properties from the Standard Model predictions. Of particular interest  
 1123 is to further constrain the peculiar self-interaction of the Higgs boson which is resonsible  
 1124 for the spontaneous breaking of the gauge symmetry of the electroweak interaction in the  
 1125 Standard Model providing masses to the mediators of the weak interaction, the  $W$  and  
 1126  $Z$  bosons. Searches for even more rare processes in the Standard Model and beyond will  
 1127 continue.

## 1128 5.7 Gas Tracking Detector Developments for Future Experiments

1129 The development of industrial methods for large-scale RPC chamber production places  
 1130 MPP in a central position for future applications of these detectors. In particular, the  
 1131 application of this technology in experiments at future high-energy electron-positron and



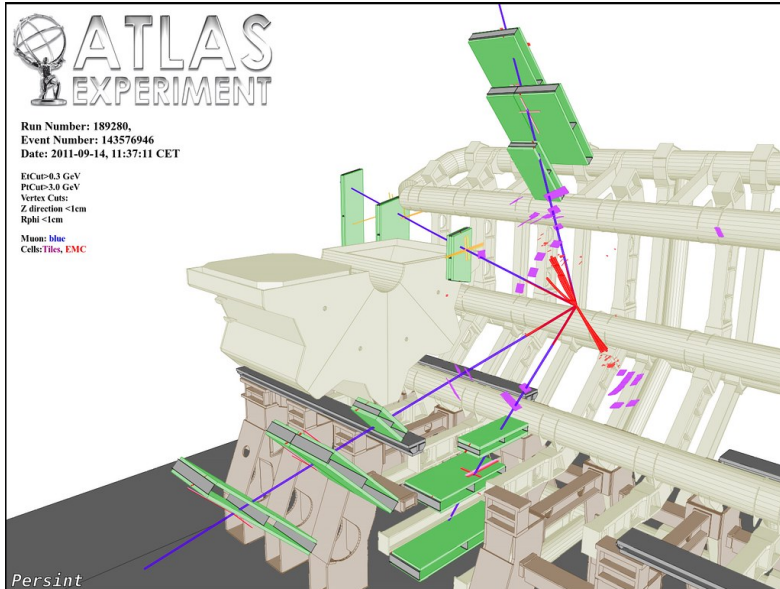


Figure 41: Cutaway electronic display of a Higgs boson decay into four muon tracks (purple lines) reconstructed in the three MDT chamber layers (green) in the barrel and one endcap of the ATLAS muon spectrometer [49]. Only the MDT chambers hit by the muons and part of the toroid magnet coils are shown.

1132 proton-proton colliders are of high interest for MPP.

1133 Gas detectors will continue to be the detector technology of choice for large area coverage  
 1134 in muon detectors and calorimeters at any collider experiment. sMDT detectors are ideal  
 1135 precision muon detectors under the even higher background radiation at future proton  
 1136 colliders [51] and can provide stand-alone muon trigger capability with high momentum  
 1137 resolution and selectivity against the vast low-energy muon background. The development  
 1138 of a muon track trigger based on the MDT and sMDT chambers in ATLAS for HL-LHC  
 1139 can be seen as a pilot project for such a future standard.

1140 RPC detectors with their high time resolution and cost effective coverage of large areas are  
 1141 needed for the detection of long-lived particles decaying at the edge of the detectors. Gas  
 1142 drift detectors containing very little scattering material are needed for the central track-  
 1143 ing detectors at electron-positron colliders to provide very high spatial and momentum  
 1144 resolution for charged particle tracks.

1145 Future high-energy collider experiments present new challenges in precision, speed and  
 1146 radiation tolerance for the detectors and their readout electronics. The MPP group started  
 1147 the development of gas tracking detectors in the framework of the conceptual studies  
 1148 for experiments at Future Circular electron-positron and proton-proton colliders at the  
 1149 highest center-of-mass energies planned at CERN and called FCC-ee [53] and FCC-hh [54],  
 1150 respectively (see chapter 5).

1151 The MPP group contributed to the conceptual design of a detector [54] for a future FCC-hh  
 1152 proton-proton collider with 100 TeV center-of-mass energy and a circumference of almost



Figure 42: Top: Detector construction facility in a temperature controlled clean room at the new MPP building on the MPG campus in Garching in operation since the beginning of 2024. Large sMDT and RPC detectors will be constructed on polished granite tables using high-precision mechanical jigs and automatized robotic devices. The automated coordinate measuring machine is visible on the right. Bottom: The glueing robot in action on the assembly table for sMDT and RPC detectors.

1153 100 km. The proton collision rate and the corresponding background rates in the detectors  
 1154 will be at least an order of magnitude higher than even at the HL-LHC. At the moment,  
 1155 only calorimeters based on liquid argon as active material (see chapter 3) can be conceived  
 1156 to withstand the harsh radiation conditions.

1157 The selection of high-energy muons from the overwhelming background even in the muon  
 1158 detector requires unprecedentedly high muon momentum resolution in real time during  
 1159 the data taking. This is a new challenge compared to the ATLAS experiment, where  
 1160 the high muon momentum resolution provided by the MDT chambers was originally only  
 1161 required in the offline muon track reconstruction.

1162 Once again, the sMDT chambers provide the ideal solution also as high-precision muon

1163 trigger detectors in combination with the central tracking detector for which a working  
1164 concept under FCC-hh conditions has yet to be found. To this end, sMDT chambers have  
1165 to measure the deflection of the muons in the magnetic field of the central tracking detector  
1166 right after their passage through the calorimeters with unprecedentedly high precision.  
1167 Deviations from vertical incidence of less than  $70\ \mu\text{m}$  have to be resolved over typically  
1168 a meter distance between two successive sMDT detector layers. As the measurement has  
1169 to be performed in real time, alignment corrections from an optical monitoring system  
1170 like in ATLAS cannot be applied. The sMDT chamber layers at FCC-hh have to be  
1171 build in monolithic pieces with perfect alignment and without deformations. This is only  
1172 possible using the sMDT technology in a monolithic design of two multi-layers of drift  
1173 tubes separated by an extraordinary stiff support frame of up to 1.7 m height and overall  
1174 better than  $20\ \mu\text{m}$  sense wire positioning accuracy [51].

1175 At the same time, the sMDT chambers have proven to provide radiation tolerance and  
1176 background rate capability which is more than sufficient for even FCC-hh conditions [51].  
1177 The sMDT readout and trigger scheme developed at MPP for the upgrade of the ATLAS  
1178 detector at HL-LHC can be directly employed also for the real-time muon direction and  
1179 momentum measurement at FCC-hh.

1180 A new facility for large-scale gas detector construction with high degree of automatization  
1181 has been created in the new institute building in Garching (Fig. 42). The construction of  
1182 a large prototype sMDT muon tracking and trigger chamber for FCC-hh is on the way  
1183 using this facility. Studies of new electrode materials and gas mixtures with low global  
1184 warming potential for RPC detectors which can tolerate high irradiation doses are on the  
1185 way.

1186 For all such detectors at future colliders, new fast, radiation hard readout electronics  
1187 with integrated circuit chips in modern chip fabrication technologies are required. In the  
1188 course of the developments for the ATLAS HL-LHC upgrade, the MPP ATLAS group  
1189 and the MPP electronics department are set up to make significant contributions to these  
1190 developments. Robert Richter from the MPP group, ATLAS MDT electronics coordinator  
1191 until the start of data taking, was indispensable for the further development of the MDT  
1192 readout electronics for HL-LHC and for future colliders and for establishing chip design  
1193 capabilities at MPP.

1194 The MPP group pioneered studies of the performance of drift tube detectors and their  
1195 readout electronics at high counting rates. The full high-rate potential of the sMDT  
1196 chambers at future colliders can only be exploited with faster readout electronics beyond  
1197 the design for the ATLAS upgrade which is already faster than the original MDT readout  
1198 electronics and more than sufficient for HL-LHC. Since more than 10 years, the MPP  
1199 ATLAS group works on the further improvement of the rate capability of gas detector  
1200 electronics, a research program which does not exist anywhere else.

1201 Fast, sophisticated trigger algorithms are under development, which can fully exploit the  
1202 information delivered by the ever more granular detectors within microseconds. The im-  
1203 plementation of neural network and other artificial intelligence algorithms on the fast  
1204 programmable real-time processors (FPGAs) in order to further improve the trigger se-

1205 lectivity in increasingly complex environment is part of the MPP reserach program.

## 1206 **6 From ATLAS to Future Colliders**

1207 The HL-LHC will significantly extend the measurement precision of the LHC for parame-  
1208 ters and rare processes in the Standard Model and the reach of searches for new phenomena  
1209 beyond the Standard Model. It is the natural extension of the LHC. In parallel, however,  
1210 the preparation for new colliders with capabilities beyond the HL-LHC has to take place as  
1211 the planning and construction time for such unprecedentedly large and complex projects,  
1212 which require world-wide collaboration, is several decades.

1213 New high-energy colliders after the HL-LHC are under discussion since even before the  
1214 approval of the LHC. Various linear electron-positron collider technolgies and, more re-  
1215 cently, also circular electron-positron colliders, have been proposed with center-of-mass  
1216 energies sufficient for resonant production of the Higgs boson at high rates. The study  
1217 of the properties of the Higgs boson with ever higher precision is considered to be one of  
1218 the most promising portals to the discovery of physics beyond the Standard Model and  
1219 answers to the many questions it still leaves open.

1220 After the revolutionary findings by the LHC experiments, the construction of such an  
1221 electron-positron "Higgs factory" is now the top priority of the High Energy Physics  
1222 community in Europe, and in the world, for the time after the HL-LHC. The design  
1223 favoured at CERN is a circular collider with about 100 km circumference which provides  
1224 a center-of-mass energy reach from the  $Z$  resonance near 90 GeV through the Higgs boson  
1225 resonance at 125 GeV upto the top quark pair production threshold around 350 GeV. It  
1226 will provide high-precision model-independent measurements of  $Z$ , Higgs and top quark  
1227 properties, measurement of the Higgs boson self coupling, and searches for new phenomena  
1228 up to very high energy scales through higher order radiative processes [52]. The required  
1229 accelerator technology and a detailed conceptual design study for such a Future Circular  
1230  $e^+e^-$  Collider (FCC-cc) [53] are already available.

1231 Afterwards, in the same tunnel, a new proton-proton (hadron-hadron) collider with center-  
1232 of-mass energy of 100 TeV could be built, using the strategy applied for the construction  
1233 of the LHC in the former LEP collider tunnel. Such a high-energy hadron collider, named  
1234 FCC-hh [54], can provide the highest precision for testing the Standard Model and ulti-  
1235 mate reach for new physics in this centuary. It would allow for a significant measurement  
1236 of the self-coupling of the Higgs boson through Higgs boson pair production and, thus,  
1237 detailed study of the electroweak symmetry breaking mechanism, and say the final word  
1238 about the particle composition of the Dark Matter in the Universe and many proposed  
1239 extensions of the Standard Model [52]. The FCC-hh is based on known accelerator tech-  
1240 nology. It requires the development of new superconducting dipole magnets which support  
1241 twice the magnetic field strenght of the LHC magnets for which a rigorous research pro-  
1242 gram is on the way.

1243 Several detector concepts exist for a future high energy  $e^+e^-$  collider covering the center-

1244 of-mass energy range from the Z resonance near 90 GeV through the Higgs resonance at  
1245 125 GeV upto the top quark pair production threshold around 350 GeV, generally called  
1246 a "Higgs Factory". In addition to highly granular calorimeters with unprecedentedly high  
1247 energy and time resolution, they require unprecedentedly high momentum resolution for  
1248 charged particles in the central tracking detector and precise muon detection over large  
1249 areas with high time resolution.

1250 The MPP ATLAS group has competence for all detector types and experience in the  
1251 realization of large-scale detector construction projects. Research and development for  
1252 innovative high-performance detector concepts for future colliders has started. World-class  
1253 detector construction facilities have been created at the new institute building where large-  
1254 volume detectors as required for future collider experiments can be built in temperature  
1255 controlled clean rooms.

1256 With the expected more than 10 times luminosity and radiation rates at FCC-hh compared  
1257 to HL-LHC, calorimetry based on liquid argon currently appears to be the only choice with  
1258 sufficient radiation hardness. A design of highly granular electromagnetic and hadronic  
1259 liquid argon calorimeters in the barrel and forward regions following the TGT concept  
1260 has been studied [37]. A similar approach may also provide a competitive solution for a  
1261 FCC-ee detector with optimum segmentation and homogeneity  $\eta$  [37], the 'turbine' being  
1262 realized in  $\phi$  rather than in  $\eta$  for an  $e^+e^-$  collider experiment.

1263 The central tracking detector at an  $e^+e^-$  collider needs to combine very high mechanical  
1264 accuracy with minimum scattering material deflecting the traversing particles in order  
1265 to achieve the unprecedentedly high required spatial resolution. The expertise from the  
1266 SMDT chambers helps in the development of a central tracking chamber for FCC-ee con-  
1267 sisting of small-diameter, so called straw drift tubes with very thin walls of low-Z material.

1268 The muon detectors of FCC-ee experiments not only need to cover large areas but also have  
1269 to provide very good time resolution for the reconstruction of tracks of long-lived particles.  
1270 The RPC detectors developed for the ATLAS upgrade at HL-LHC are a competitive choice  
1271 for which the MPP ATLAS group has extensive experience. Novel types of RPC chambers  
1272 with even higher time resolution of better than 100 ps may be used for time-of-flight  
1273 measurements and particle identification.

1274 For muon detection and triggering at FCC-hh, SMDT detectors with novel fast readout  
1275 electronics under development are at present the only conceivable choice for most of the  
1276 solid angle.

1277 The MPP ATLAS group is well prepared for challenges in detector design and construction  
1278 for future high-energy lepton and hadron colliders in the next several decades and related  
1279 applications in other experiments promising to help understand the physics beyond the  
1280 Standard Model.



1281 **References**

- 1282 [1] J. Kemmer, “Fabrication of low noise silicon radiation detectors by the planar pro-  
1283 cess,” Nucl. Instrum. Meth. **169** (1980), 499-502
- 1284 [2] S. R. Amendolia, G. Batignani, F. Bedeschi, E. Bertolucci, L. Bosisio, C. Bradaschia,  
1285 M. Budinich, F. Fidecaro, L. Foa and E. Focardi, *et al.* “A Multielectrode Silicon  
1286 Detector for High-energy Physics Experiments,” Nucl. Instrum. Meth. **176** (1980),  
1287 457
- 1288 [3] B. Hyams, U. Kotz, E. Belau, R. Klanner, G. Lutz, E. Neugebauer, A. Wylie and  
1289 J. Kemmer, “A Silicon Counter Telescope to Study Shortlived Particles in High-energy  
1290 Hadronic Interactions,” Nucl. Instrum. Meth. **205** (1983), 99-105
- 1291 [4] S. Barlag *et al.* [ACCMOR], “Measurement of the Masses and Lifetimes of the  
1292 Charmed Mesons  $D^0$ ,  $D^+$  and  $D_s^+$ ,” Z. Phys. C **46** (1990), 563-568
- 1293 [5] S. Barlag *et al.* [ACCMOR], “Precise Determination of the Lifetime of the Charmed  
1294 Baryon  $\Lambda(c)$ ,” Phys. Lett. B **218** (1989), 374
- 1295 [6] G. Lutz, W. Buttler, H. Bergmann, P. Holl, B. J. Hosticka, P. F. Manfredi and  
1296 G. Zimmer, “LOW NOISE MONOLITHIC CMOS FRONT END ELECTRONICS,”  
1297 Nucl. Instrum. Meth. A **263** (1988), 163
- 1298 [7] B. Mours *et al.* “The Design, construction and performance of the ALEPH silicon  
1299 vertex detector,” Nucl. Instrum. Meth. A **379** (1996), 101-115
- 1300 [8] D. Buskulic *et al.* [ALEPH], “A Precise measurement of the average  $b$  hadron life-  
1301 time,” Phys. Lett. B **369** (1996), 151-162
- 1302 [9] D. Buskulic *et al.* [ALEPH], “Measurement of the anti- $B^0$  and  $B^-$  meson lifetimes,”  
1303 Phys. Lett. B **307** (1993), 194-208 [erratum: Phys. Lett. B **325** (1994), 537-538]
- 1304 [10] D. Buskulic *et al.* [ALEPH], “Measurement of the  $B_s^0$  lifetime,” Phys. Lett. B **322**  
1305 (1994), 275-286
- 1306 [11] D. Buskulic *et al.* [ALEPH], “Measurements of the  $b$  baryon lifetime,” Phys. Lett. B  
1307 **357** (1995), 685-698
- 1308 [12] D. Buskulic *et al.* [ALEPH], “Observation of the time dependence of  $B_d^0$  - anti- $B_d^0$   
1309 mixing,” Phys. Lett. B **313** (1993), 498-508
- 1310 [13] D. Buskulic *et al.* [ALEPH], “A Precise measurement of Gamma ( $Z \rightarrow b\bar{b}$ ) / Gamma  
1311 ( $Z \rightarrow$  hadrons),” Phys. Lett. B **313** (1993), 535-548
- 1312 [14] A. Ahmad, Z. Albrechtskirchinger, P. P. Allport, J. Alonso, L. Andricek, R. J. Apsi-  
1313 mon, A. J. Barr, R. L. Bates, G. A. Beck and P. J. Bell, *et al.* “The Silicon microstrip  
1314 sensors of the ATLAS semiconductor tracker,” Nucl. Instrum. Meth. A **578** (2007),  
1315 98-118

- 1316 [15] F. Campabadal, C. Fleta, M. Key, M. Lozano, C. Martinez, G. Pellegrini, J. M. Rafi,  
1317 M. Ullan, L. G. Johansen and B. Mohn, *et al.* “Design and performance of the  
1318 ABCD3TA ASIC for readout of silicon strip detectors in the ATLAS semiconduc-  
1319 tor tracker,” Nucl. Instrum. Meth. A **552** (2005), 292-328
- 1320 [16] J. Kemmer and G. Lutz, “NEW DETECTOR CONCEPTS,” Nucl. Instrum. Meth.  
1321 A **253** (1987), 365-377
- 1322 [17] J. Kemmer, G. Lutz, U. Prechtel, K. Schuster, M. Sterzik, L. Struder and T. Zie-  
1323 mann, “Experimental Confirmation of a New Semiconductor Detector Principle,”  
1324 Nucl. Instrum. Meth. A **288** (1990), 92-98
- 1325 [18] F. Abudinén *et al.* [Belle-II], “Precise measurement of the  $D^0$  and  $D^+$  lifetimes at  
1326 Belle II,” Phys. Rev. Lett. **127** (2021) no.21, 211801 [arXiv:2108.03216 [hep-ex]].
- 1327 [19] I. Adachi *et al.* [Belle-II], “Precise Measurement of the  $D_s^+$  Lifetime at Belle II,”  
1328 Phys. Rev. Lett. **131** (2023) no.17, 171803
- 1329 [20] F. Abudinén *et al.* [Belle-II], “Measurement of the  $\Lambda_c^+$  Lifetime,” Phys. Rev. Lett.  
1330 **130** (2023) no.7, 071802
- 1331 [21] F. J. Abudinen *et al.* [Belle-II], “Measurement of the  $\Omega_c^0$  lifetime at Belle II,” Phys.  
1332 Rev. D **107** (2023) no.3, L031103
- 1333 [22] S. Bähr et al., Hep-ex arXiv:2402.14962 (submitted to NIMA)
- 1334 [23] H.J.Behrend et al., CELLO-A New Detector at PETRA, Physica Scripta Vol. 23  
1335 (1981) 610-622.
- 1336 [24] Ref. measurement of the tau branching ratios
- 1337 [25] H1 Collab., I.Abt et al. The H1 Detector at HERA, DESY preprint 93-103 (1993).
- 1338 [26] The H1 Calorimeter Group, B.Andrieu et al. The H1 Liquid Argon Calorimeter Sys-  
1339 tem, DESY preprint 93-078 (1993).
- 1340 [27] Ref. to longitudinal structure function of the proton
- 1341 [28] J. K. Köhne, C. Kiesling et al., Nucl. Instrum. Meth. A 389 (1997) 128.
- 1342 [29] C. Adloff et al., Phys. Lett. B483 (2000) 23.
- 1343 [30] P. Norton et al., ”The ASCOT Detector at the LHC–Expression of Interest”, proceed-  
1344 ings of the General Meeting on LHC Physics and Detectors, Evian-les-Bains, March  
1345 1992.
- 1346 [31] H. Brettel et al., Conceptual Design of a ’Thin Gap Turbine’ Calorimeter for the  
1347 LHC, MPI Report 92-15 (1992).
- 1348 [32] RD33 coll., Study of the TGT Concept for Liquid Argon Calorimetry,  
1349 CERN/DRDC/94-8.
- 1350 [33] B. Aubert et al., (RD3 Collaboration), Liquid Argon Calorimetry with LHC-  
1351 Performance Specification, CERN/DRDC/90-31 (1990).

- 1352 [34] C. Berger et al., A Highly Segmented and Compact Liquid Argon Calorimeter for the  
1353 LHC,
- 1354 [35] ATLAS Letter of Intent, CERN/LHCC/92-4 (1992). CERN/DRDC 92-41,  
1355 DRDC/P44 (1992).
- 1356 [36] ATLAS Technical Proposal, CERN/LHCC/94-43, LHCC/P2, (1994).
- 1357 [37] M. Aleksa et al., Calorimeters for the FCC-hh, CERN/FCC-PHYS-2019-0003 (2019).
- 1358 [38] H.J. Behrend et al. Model independent limits on  $\Lambda_{QCD}$  from  $e^+e^-$  annihilation in the  
1359 energy range from 14 to 46 GeV, Z.Phys.C- Particles and Fields,44,63-69 (1989) and  
1360 references therein.
- 1361 [39] ATLAS collaboration, G. Aad et al., "The ATLAS Experiment at the Large Hadron  
1362 Collider", Journal of Instrumentation **3** (2008) S08003.
- 1363 [40] ATLAS collaboration, G. Aad et al., "ATLAS Muon Spectrometer Technical Design  
1364 Report", CERN report, CERN/LHCC 97-22, June 1997.
- 1365 [41] F. Bauer et al., "Construction and Test of the Precision Drift Chambers for the  
1366 ATLAS Muon Spectrometer", IEEE Transactions on Nuclear Science Vol. 48, No. 3  
1367 (2001) 302.
- 1368 [42] Ph. Schwegler, O. Kortner, H. Kroha, R. Richter, "Improvement of the L1 trigger  
1369 for the ATLAS Muon Spectrometer at high luminosity", Nuclear Instruments and  
1370 Methods **A 718** (2013) 245.
- 1371 [43] H. Kroha, R. Fakhroutdinov, A. Kozhin, New High-Precision Drift Tube Chambers  
1372 for the ATLAS Muon Spectrometer, Journal of Instrumentation **12** (2017) C06007.
- 1373 [44] M. De Matteis, F. Resta, R. Richter, H. Kroha, M. Fras, Y. Zhao, A. Baschirotto,  
1374 "Performance of the New Amplifier-Shaper-Discriminator Chip for the ATLAS MDT  
1375 Chambers at the HL-LHC", Journal of Instrumentation **11.02** (2016) C02087.
- 1376 [45] ATLAS collaboration, "Technical Design Report for the Phase-II Upgrade of the AT-  
1377 LAS Muon Spectrometer", CERN report, CERN-LHCC-2017-017, September 2017.
- 1378 [46] ATLAS collaboration, "Technical Design Report for the Phase-II Upgrade of the  
1379 ATLAS TDAQ System", CERN report, CERN-LHCC-2017-020, September 2017.
- 1380 [47] O. Kortner, H. Kroha, D. Soyk, T. Turkovic, "Industrialization of resistive plate cham-  
1381 ber production", Nuclear Instruments and Methods **A 1044** (2022) 167481.
- 1382 [48] ATLAS collaboration, G. Aad et al., "Observation of a new particle in the search  
1383 for the Standard Model Higgs boson with the ATLAS detector at the LHC", Physics  
1384 Letters **B 716** (2012) 1.
- 1385 [49] ATLAS collaboration, ATLAS collision event display from 14 September 2011.
- 1386 [50] ATLAS collaboration, G. Aad et al., "Measurement of the Higgs boson mass in the  
1387  $H \rightarrow ZZ^* \rightarrow 4\ell$  decay channel using  $139 \text{ fb}^{-1}$  of  $\sqrt{s} = 13 \text{ TeV}$  pp collisions recorded  
1388 by the ATLAS detector at the LHC", Physics Letters **B 843** (2023) 137880.

- 1389 [51] G. Eberwein, O. Kortner, S. Kortner, H. Kroha, R. Richter, E. Voevodina, "High-  
1390 Precision Large-Area Muon Tracking and Triggering with Drift Tube Chambers at  
1391 Future Colliders", Nuclear Instruments and Methods **A 1044** (2022) 167482.
- 1392 [52] FCC collaboration, A. Abada et al., "FCC Physics Opportunities", Future Circular  
1393 Collider Conceptual Design Report, Volume 1, The European Physical Journal **C 79**  
1394 (2019) 474.
- 1395 [53] FCC collaboration, A. Abada et al., "FCC-ee: The Lepton Collider", Future Circular  
1396 Collider Conceptual Design Report, Volume 2, The European Physical Journal Special  
1397 Topics, Vol. 228 (2019) 261.
- 1398 [54] FCC collaboration, A. Abada et al., "FCC-hh: The Hadron Collider", Future Circular  
1399 Collider Conceptual Design Report, Volume 3, The European Physical Journal Special  
1400 Topics, Vol. 228 (2019) 755.

1401 <https://sharelatex.gwdg.de/project/65fc06ebd022a33edede3d55>